

# Electron- and Charge-Transfer Reactions within Zeolites

Kyung Byung Yoon

Department of Chemistry, Sogang University, Seoul 121-742, Korea

Received June 30, 1992 (Revised Manuscript Received October 13, 1992)

## Contents

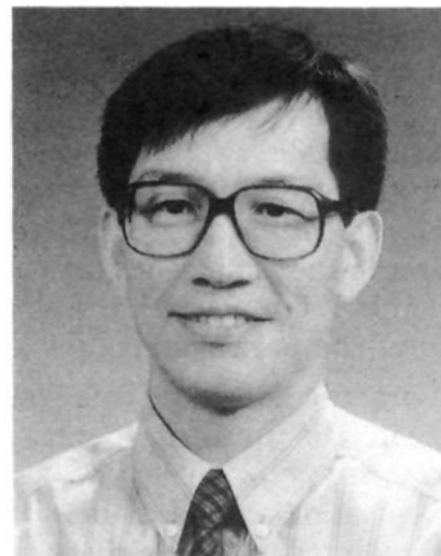
I. Introduction	321
II. Charge-Transfer Interactions between Intercalated Molecules	322
A. Stepwise Assembly of Pyridinium-Arene CT Complexes	322
1. Intracavity Assembly	322
2. Visual Probes for Shape Selectivity	325
B. Stepwise Assembly of Pyridinium Iodide CT Salts	326
III. Electron Transfer between Intercalated Molecules	328
A. Photoassisted Electron Transfer	328
B. Thermal Electron Transfer	330
1. Superoxide Electron Transfer	330
2. Oxidation of Organic Compounds with Metal Ions	332
3. Redox Reactions between Inorganic Compounds	332
IV. Zeolite Framework as Electron Donor and Acceptor	332
A. Zeolite Framework as Electron Acceptor	332
1. Induction by Thermal Treatment	332
2. Radiation-Induced Acceptor Property	337
B. Zeolite Framework as Electron Donor	337
1. Induction by Thermal Treatment	337
2. Radiation-Induced Donor Property	337
V. Acknowledgments	338
VI. References	338

## I. Introduction

Thermal or photochemical charge transfer (CT) activation of the precursor complexes<sup>1</sup> [electron donor-acceptor (EDA) or CT complexes] from donor (D) to acceptor (A) is a primary step for a variety of reactions (eq 1).<sup>2</sup> Accordingly, extensive studies have been carried



out to elucidate the precise nature of CT processes.<sup>3</sup> In general, charge-transfer reactions have been more often carried out in solution, where the effect of solvation is substantial on governing not only the complexation of the precursor complexes<sup>4</sup> but also the subsequent follow-up reactions which ultimately determine the overall efficiency and selectivity of the CT processes.<sup>3</sup> However, despite its importance, studies designed to delineate the solvation effects on such reactions are rather limited, presumably due to the featureless and poorly



Kyung Byung Yoon was born on March 10, 1956, in Seoul, Korea. In 1979 he received his B.S. from the Department of Chemistry, Seoul National University. In 1981 he obtained his M.S. from the Department of Chemistry, Korea Advanced Institute of Science, Seoul, where his Research Advisor was Professor Hakze Chon and his research field was hydrogenation reactions over metal-doped zeolites. From 1981 to 1984 he was employed by Chon Engineering Co. Ltd., Seoul. There he gained experience in catalyst design and the engineering of chemical process plants and the design of pilot plants for zeolite synthesis. In 1989 he earned his Ph.D. in inorganic chemistry from the Department of Chemistry, University of Houston, Houston, Texas, where his Research Advisor was Professor Jay K. Kochi and his research field was reactions in zeolites under mild conditions. From 1989 to the present he has been an Assistant Professor of Chemistry, at Sogang University, where he is continuing his zeolite research.

organized nature of the solvent cages.<sup>5</sup> In this regard, a variety of CT and electron-transfer reactions have been explored in organized media<sup>6</sup> with the hope of broadening our knowledge about the nature of solvation shells as well as CT processes.

Zeolites are crystalline aluminosilicate minerals with the general formulation  $M_x[(AlO_4)_x(SiO_4)_y] \cdot n(H_2O)$  which are widely used as sorbents, ion exchangers, catalysts, and catalyst supports.<sup>7</sup> Their structure is based on a three-dimensional network of  $[AlO_4]^{5-}$  and  $[SiO_4]^{4-}$  tetrahedra which are linked to each other via doubly bridging oxygen atoms. As each aluminum atom incorporated into the framework leads to the presence of one excess negative charge, charge-compensating cations ( $M^+$ ) must be introduced into the structure. The framework structures create regular arrays of very open void spaces often called cages or channels, depending on the shape of the pores (cavities) which are normally filled with cations and water. These cations are not covalently bound to the zeolite framework; therefore, they can be readily substituted with a variety of other cations via conventional aqueous ion exchange. A proton ( $H^+$ ) is one of the most frequently exchanged cations which gives rise to the zeolite Brønsted acidity. The cavity-filling water molecules

are readily lost and regained reversibly without damaging the framework structure. When dehydrated, other guest molecules can occupy the void spaces as long as the interior spaces are large enough and the aperture sizes allow passage of the substrates. Typically, the aperture size of zeolite pores ranges from 3 to 8 Å, and the inner diameter of interior spaces from 5 to 13 Å. For a given type of zeolites, characteristic properties also arise from the variation of the silicon to aluminum ratio (Si/Al), the type of exchanged cations, and the condition of pretreatment. The silicon to aluminum ratio eventually determines the number of total exchangeable cation sites. The most frequently appearing zeolites in this article are zeolite-A (A), zeolite-X (X), zeolite-Y (Y), mordenite (M), ZSM-5, zeolite-L (L), and sodalite. The framework structures of zeolites X and Y are identical, but they have different silicon to aluminum ratios; X = 1–1.5 and Y = 1.5–3. Figure 1 represents the framework structures of these zeolites, and Table I summarizes the size, shape, and dimensionality of the pore systems for these zeolites.

A variety of organic and inorganic transformations can occur within the uniform pores of molecular dimension.<sup>7</sup> Accordingly, zeolites have been extensively used as prototypical organized media for a variety of reactions since zeolite pores are akin to solvent cages.<sup>8</sup> In addition to this principal similarity of zeolite pores to solvent shells, there are unique features that only zeolite pores can provide. First of all, zeolite pores are extremely rigid and distinctively shaped<sup>7</sup> in striking contrast to the relatively soft and featureless solvent shells. Secondly, the negatively charged surface of aluminosilicate frameworks provides a polar environment which can be further modified by varying the number and type of charge compensating cations via conventional ion exchange.<sup>7</sup> Thirdly, the ion exchange with cations of various sizes (shapes) and valence charges can be effectively utilized for the fine control of zeolite pore sizes.<sup>7,9</sup> In addition, the zeolite framework itself possesses amphoteric properties<sup>10–13</sup> of both electron donors and acceptors which render intrazeolite chemistry even more versatile.

In this regard, many interesting reactions including electron- and charge-transfer reactions have been explored within zeolite pores, and the results have often been unique compared to those in solution. In return, invaluable information regarding the properties of the zeolite surface has been obtained from such studies.

This article is primarily concerned with recent progress on electron- and charge-transfer reactions in zeolites out of those innumerable interesting reactions that have been performed within zeolites. The reactions involve charge-transfer complexation between electron donors (arenes and iodides) and acceptors (*N*-methylpyridinium ions) and their photostimulation leading to an electron transfer. A variety of photo-electron-transfer reactions associated with the excited states of tris(2,2'-bipyridyl)ruthenium(II) Ru(bpy)<sub>3</sub><sup>2+</sup> and a porphyrin complex of Zn(II) are described. Superoxide electron-transfer reactions from various immobilized, unstable organic and inorganic compounds within zeolite pores are summarized. Many interesting reactions that take full advantage of the remarkable, intrinsic properties of zeolites of readily oxidizing adsorbed substrates and stabilizing the highly unstable

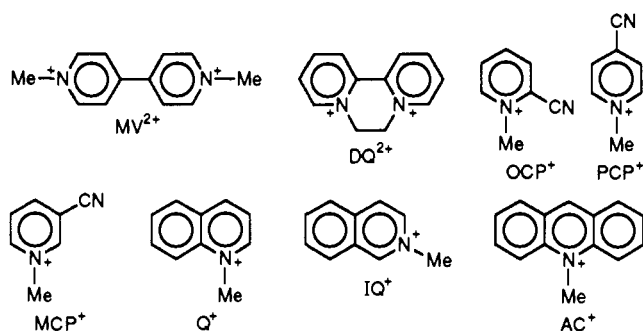
species generated in these reactions are described in depth. These reactions include formation of various organic cation radicals, polymerization, hole-catalyzed pericyclic reactions, and formation of alkali metal ionic clusters that can be considered as electron-trapping devices in some zeolites. In the final section, radiation ( $\gamma$ - or X-rays) induced formation of cation or anion radicals of various substrates is described.

## II. Charge-Transfer Interactions between Intercalated Molecules

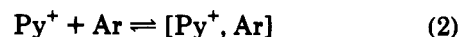
### A. Stepwise Assembly of Pyridinium–Arene CT Complexes

#### 1. Intracavity Assembly

A series of aromatic charge-transfer complexes was assembled shape selectively<sup>9</sup> within zeolite-Y supercages doped with mono- and dipyridinium acceptors.<sup>14,15</sup> The pyridinium acceptors were methylviologen, MV<sup>2+</sup>; diquat, DQ<sup>2+</sup>; *N*-methylquinolinium, Q<sup>+</sup>; *N*-methylisoquinolinium, IQ<sup>+</sup>; *N*-methylacridinium, AC<sup>+</sup>; *N*-methyl-2-cyanopyridinium, MCP<sup>+</sup>; and *N*-methyl-4-cyanopyridinium, PCP<sup>+</sup>. These have been known as electron acceptors



in solution, i.e.,



As a primary step for the formation of intrazeolite charge-transfer complexes, the acceptor ions from the corresponding halide salts were readily incorporated into zeolite-Y via aqueous ion exchange of charge-compensating cations (typically Na<sup>+</sup>). The maximum number of acceptor ions that could be incorporated into zeolite-Y was limited by the constrained space of the supercages. The exchanged acceptors within zeolite-Y were identified by both solid-state <sup>13</sup>C NMR and the diffuse reflectance UV–vis spectra of the colorless samples, except the AC<sup>+</sup>-doped yellow zeolite which was also greenish fluorescent, due to the intrinsic properties of the ion. The reversible ion exchange of the organic cations by excess Na<sup>+</sup> further confirmed that the acceptors remained intact during the ion exchange. The use of cationic acceptor molecules had many advantages, since the incorporation and control of the degree of doping into zeolite-Y could be easily achieved by simple ion exchange, and the acceptors did not leach out during the subsequent intercalation of arene donors in organic solvents.

For the formation of charge-transfer complexes within the supercages, partially doped zeolites (typically 0.7–1.0 ion per each supercage) were evacuated, followed

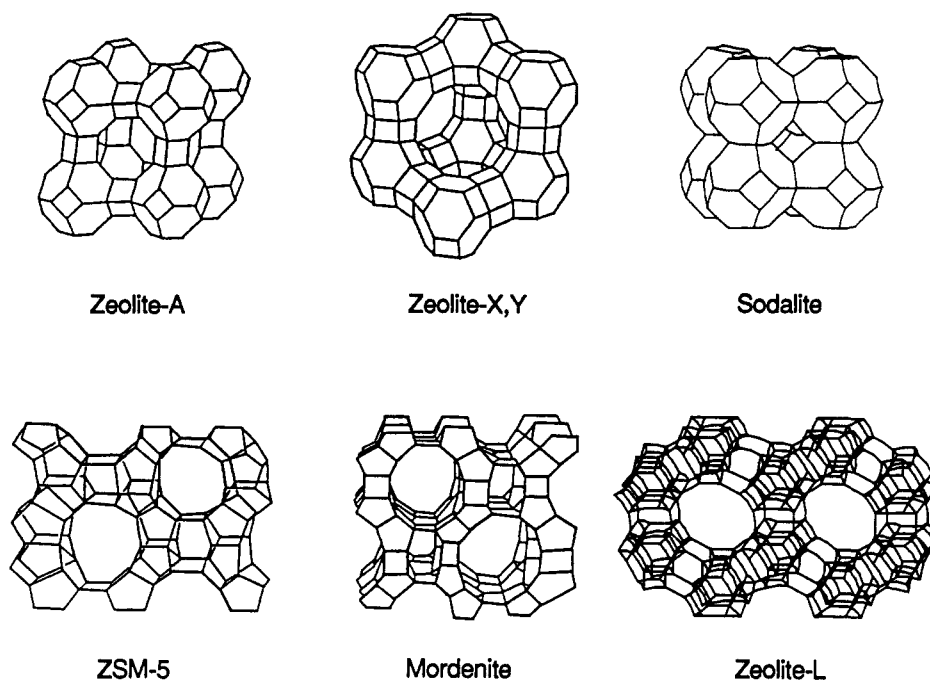


Figure 1. Structures of zeolites: zeolite-A, zeolite-X,Y, sodalite, ZSM-5, mordenite, and zeolite-L.

Table I. Size of Pore Openings and Dimensionality of the Pore System for Selected Zeolites That Frequently Appeared in the Text<sup>a</sup>

zeolite	effective window size, Å	pore shape (size, Å)	dimensionality
A	4.2	cage (11.4)	three
X,Y	7.4	cage (11.8)	three
sodalite	2.3	cage (6.6)	three
ZSM-5	5.3 × 5.6, 5.1 × 5.5	channel	two, interconnecting
mordenite	7.0 × 6.7, 2.6 × 5.7	channel	two, interconnecting
L	7.1	lobe (7.5)	single

<sup>a</sup> Meier, W. M.; Olson, D. H. In *Atlas of Zeolite Structure Types*, 2nd revised ed.; Butterworths: Cambridge, 1987, and from ref 7a.

by the gradual increase of the temperature up to 100 °C<sup>16</sup> over a period of 10 h, to remove water from the cavities. The CT complexation was then effectively carried out by exposing the dried, doped zeolites to hexane solutions of various arenes in a dry atmosphere. The colorless zeolites then immediately developed intense colors of yellow, orange, purple, and even green, depending on the combination of the doped acceptors and arene donors. However, the supernatant solutions remained colorless, indicating that the coloration occurs solely on the zeolite powders. The subsequent gas chromatographic analyses of the supernatant solutions revealed the loss of significant amounts of arene donors from the solution, indicating that the intercalation of arene donors into doped zeolites had indeed occurred. The solid-state <sup>13</sup>C NMR spectra of the colored zeolite samples showed the corresponding composite peaks of both pyridinium acceptors and arene donors.

The diffuse reflectance spectra of the colored samples revealed well resolved, new absorption bands as represented in Figure 2A for the brightly colored MVY (zeolite-Y doped with MV<sup>2+</sup>) which was treated with arenes as indicated. The developed colors were then ascribed to CT interaction between the acceptors and

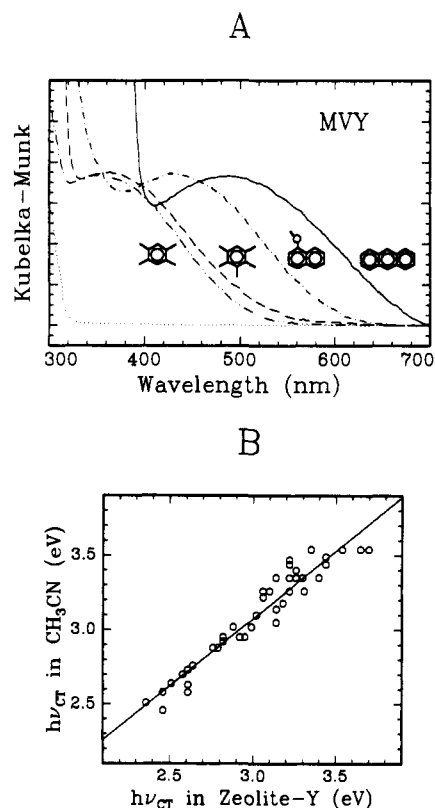


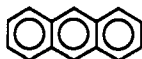
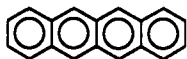



Figure 2. (A) Diffuse reflectance spectra of colored zeolites from the exposure of MVY to arenes (as indicated). (Untreated MVY before exposure to arene is shown as a dotted line.) (B) Linear relationship between the charge transfer spectra ( $h\nu_{CT}$ ) of various arene-pyridinium complexes in zeolite-Y and in acetonitrile solution.<sup>16</sup>

arenes within zeolite-Y supercages from the close similarity of the new absorption bands of the colored zeolites and the authentic CT bands of the corresponding complexes in solution as represented by the linear correspondence in Figure 2B. Table II summarizes the absorption maxima ( $\lambda_{max}$ ) of the new bands obtained from MV<sup>2+</sup>- and DQ<sup>2+</sup>-doped zeolite-Y in comparison

Table II. Diffuse Reflectance Spectra of Charge-Transfer Complexes in Zeolite-Y and Effect of Aromatic Donors<sup>15</sup>

	arene donor	IP <sup>a</sup>	zeolite-Y <sup>b</sup>		Al <sub>2</sub> O <sub>3</sub> : <sup>c</sup> MV <sup>2+</sup>	sol.: <sup>d</sup> MV <sup>2+</sup>
			MV <sup>2+</sup>	DQ <sup>2+</sup>		
	1,2,4,5-Me <sub>4</sub>	8.05	380	390	~360	~360
	1-Me-4-MeO	8.18	370	380	~370	~365
	1,4-(MeO) <sub>2</sub>	7.90	400	420	410	406
	Me <sub>5</sub>	7.92	395	400	~370	357
	Me <sub>6</sub>	7.85	none	none	~400	385
		8.12	380	390	~360	~360
	1-Me	7.96	400	410	~380	~380
	1,4-Me <sub>2</sub>	7.78	425	430	~410	~410
	1-MeO	7.72	430	438	410	410
	1,4-(MeO) <sub>2</sub>	7.50	none	none	480	480
	2,6-(MeO) <sub>2</sub>	7.58	450	490	~440	~430
		7.43	490	500	475	472
	9-CHO	7.84	405	410	420	~390
	9-Me	7.25	518	528	515	504
	9,10-Me <sub>2</sub>	7.11	none	none	520	526
	2- <i>t</i> -Bu	~7.3	none	505	490	484
	9-Ph	7.18	none	none	~480	~500
		6.97	none	600	~590	
		6.61	none	none	~600	

<sup>a</sup> Ionization potential of Ar in eV. <sup>b</sup>  $\lambda_{CT}$  (nm) as described in the text. <sup>c</sup> Alumina (10%) suspension. <sup>d</sup> Absorption spectrum of arene CT complex with 75mM (MV<sup>2+</sup>(PF<sub>6</sub><sup>-</sup>)<sub>2</sub> in acetonitrile solution.

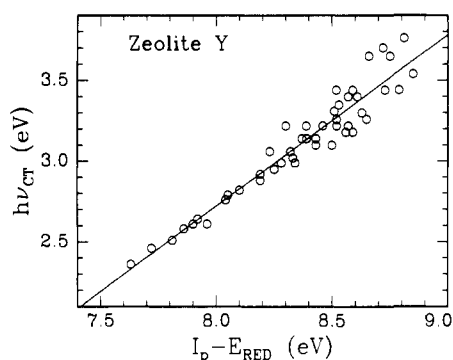


Figure 3. Mulliken relationship of the charge-transfer bands ( $h\nu_{CT}$ ) from the exposure of MVY, DQY, PCPY, and OCPY to various arene donors listed in Table II.<sup>15</sup>

with those in alumina suspension and acetonitrile solution.

The charge-transfer nature of the colors that appeared in zeolite-Y was further confirmed by the Mulliken<sup>17</sup> relationship in the plot of the absorption maxima ( $h\nu_{CT}$ ) with the ionization potential (IP) of the aromatic donors and the acceptor strength ( $E^{\circ}_{red}$ ) of the pyridinium ions which was given as

$$h\nu_{CT} = 1.06(IP - E^{\circ}_{red}) - 5.75 \quad (3)$$

with a correlation factor  $R = 0.96$  as shown in Figure 3.

Since the crystal structure of MV<sup>2+</sup>-2,6-dimethoxynaphthalene CT complex revealed a face-to-face planar interaction between the adjacent ring systems as shown in Figure 4, a similar planar interaction was inferred for the structures of CT complexes within zeolite-Y supercages as depicted in Figure 5.

The nature of the solvent greatly affected the efficiency of donor intercalation. *n*-Hexane was singularly effective as the solvent of choice for the intercalation of arene donors as represented in Table III. The branched and higher homologues isooctane

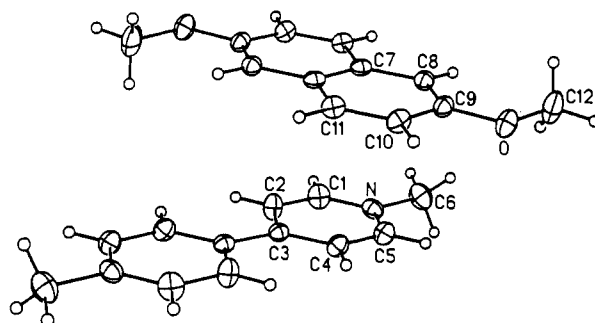


Figure 4. ORTEP perspective showing the cofacial arrangement of MV<sup>2+</sup> acceptor and 2,6-dimethoxynaphthalene donor in the 1:1 charge transfer complex. PF<sub>6</sub><sup>-</sup> is not included for clarity.<sup>15</sup>

and *n*-dodecane were significantly less effective. Chlorinated solvents were generally less effective than alkanes. Of those chlorinated solvents in the table, the efficacy increased with decrease of dielectric constants in the order CH<sub>2</sub>Cl<sub>2</sub> < CHCl<sub>3</sub> << CCl<sub>4</sub>. The uptake of donors from aromatic solvents, ethers (tetrahydrofuran), and polar solvents such as acetonitrile was ineffective. In an extreme case, the moist, undried zeolites were unable to develop colors with arenes. The results implied that the desorption of the solvent molecules out of and adsorption of arene substrates into zeolite pores should occur simultaneously.

The intercalation of arene donors into doped zeolites could also be effected in the complete absence of solvent. For example, the mere addition of liquid arene donors to doped zeolites led to brilliantly colored zeolites with somewhat greater intensity than those obtained from hexane solution. Furthermore, the direct exposure of solid arene crystals (e.g., durene, pentamethylbenzene, naphthalene, and anthracene) to doped zeolites in a closed vessel led to the characteristic charge-transfer coloration. The solid-state intercalation of arene donors into doped zeolites was, in fact, most effective for those

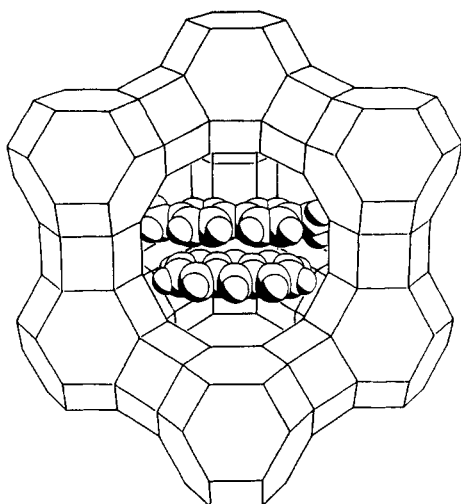


Figure 5. Pictorial representation of the "fit" within the zeolite-Y supercage of anthracene and methylviologen dication drawn to scale as parallel donor-acceptor pairs according to the CT structure in Figure 4.<sup>15</sup>

Table III. Solvent Effect on Arene Intercalation into Zeolite-Y<sup>15</sup>

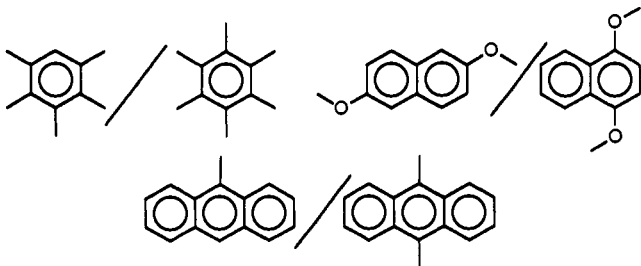
solvent	$\epsilon^a$	durene <sup>b</sup>		1-methylnaphthalene <sup>b</sup>	
		MV(1.0)Y	NaY	MV(1.0)Y	NaY
dichloromethane	9.08	0.03 (0.1)	<0.01 (0.0)	0.03 (0.1)	0.00 (0.0)
chloroform	4.81	0.13 (0.2)	0.17 (0.3)	0.18 (0.3)	0.26 (0.4)
carbon tetrachloride	2.24	0.46 (0.8)	0.86 (1.4)	0.68 (1.2)	1.11 (1.8)
<i>n</i> -hexane	1.89	0.81 (1.4)	0.84 (1.3)	1.10 (1.9)	1.30 (2.1)
isooctane	1.94	0.56 (1.0)	0.98 (1.6)	0.53 (0.9)	1.41 (2.2)
<i>n</i> -dodecane	2.01	0.35 (0.6)	1.05 (1.7)	0.57 (1.0)	1.44 (2.3)
benzene	2.28	0.15 (0.3)	0.14 (0.2)	0.12 (0.2)	0.11 (0.2)
tetrahydrofuran	7.58	<0.01 (0.0)	<0.11 (0.0)	<0.01 (0.0)	<0.01 (0.0)
acetonitrile	35.7	<0.01 (0.0)	<0.11 (0.0)	<0.01 (0.0)	<0.01 (0.0)

<sup>a</sup> Dielectric constant. <sup>b</sup> Arene intercalated into the zeolite at 25 °C (mmol/g); occupancy in parentheses (molecules per supercage).

arenes that have sufficient vapor pressures at ambient temperature.

## 2. Visual Probes for Shape Selectivity

The intrazeolite formation of CT complexes also served as a unique visual probe to monitor zeolite shape selectivity. Thus, the remarkable size (shape) exclusion of hexamethylbenzene, 1,4-dimethoxynaphthalene, and 9-phenyl- and 9,10-dimethylantracene, but not the slightly smaller yet closely related arenes as pentamethyl, 2,6-dimethoxy, and 9-methyl isomers (see below), was observed during the intercalation of most of the arenes listed in Table II into doped zeolite-Y.



Such a dramatic distinction of arene sizes led to the conclusion of the shape selectivity of zeolite hosts. The fact that the bright colors developed on doped zeolites arise from various CT complexes encapsulated within

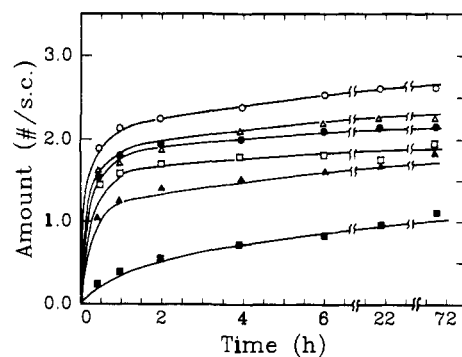


Figure 6. Time profile for the intercalation of *p*-methoxytoluene (O),  $\alpha$ -methylnaphthalene ( $\Delta$ ), and 9-methylantracene ( $\square$ ) from hexane into NaY (open symbols) and MV(1.0)Y (filled symbols).<sup>15</sup>

Table IV. Synergistic Effects of Donor and Acceptor Size (Shapes) for CT Complex Formation in Zeolite-Y<sup>15</sup>

acceptor <sup>a</sup>	donor <sup>b</sup>			
MV <sup>2+</sup> (1.0)	1.21 (2.1)	0.87 (1.5)	0.56 (1.0)	0.19 (0.3) <sup>c</sup>
DQ <sup>2+</sup> (0.8)	1.36 (2.3)	1.11 (1.9)	0.72 (1.2)	0.33 (0.6)
AC <sup>+</sup> (0.7)	1.45 (2.5)	1.24 (2.2)	0.86 (1.5)	0.48 (0.8)
Q <sup>+</sup> (0.8)	1.20 (2.0)	1.02 (1.7)	0.86 (1.5)	0.43 (0.7)
IQ <sup>+</sup> (0.8)	1.27 (2.2)	1.03 (1.8)	0.95 (1.6)	0.47 (0.8)
Na <sup>+</sup> (0.0)	1.67 (2.7)	1.37 (2.2)	1.17 (1.9)	0.70 (1.1)

<sup>a</sup> Acceptor doping in parentheses (molecules per supercage).

<sup>b</sup> Arene intercalated from hexane solution into zeolite-Y (mmol/g); occupancy in parentheses (molecules per supercage). <sup>c</sup> Only after continuous slurring for 6 h.

zeolite pores was further established by the measured uptake of arene donors by gas chromatographic analysis under a standard set of conditions. The analysis also revealed that the rates of arene uptake were generally complete within 30 min, while the uptake of the relatively large arene 9-methylantracene into doped zeolite was somewhat slower in accordance with visual observation. The typical time profile of arene uptake into Y (both doped and undoped) is represented in Figure 6. As was expected, the amounts of arene intercalation into undoped zeolites were observed to be higher than into doped samples. A similar time profile was also observed during the solvent extraction of the arenes from the colored zeolites. The sharply delineated kinetic behavior of arene uptake and extraction, depending on the sizes of arenes, contributed to render intracavity CT complexation as a unique probing method of zeolite shape selectivity.

The fine-tuning mode of zeolite shape selectivity was also demonstrated by the synergistic effects of donor and acceptor sizes as summarized in Table IV. The related synergistic effects of donor sizes and acceptor loading is illustrated in Figure 7. Since the sizes of pyridinium acceptors were significantly larger than most of the metal ions, the effects of the sizes and the degree of acceptor loadings on zeolite shape selectivity via intrazeolite CT complexation turned out to be quite a bit more dramatic than the related results where metal ions have been employed to shape the pores.<sup>9</sup> The viability of the visual probe method of zeolite shape

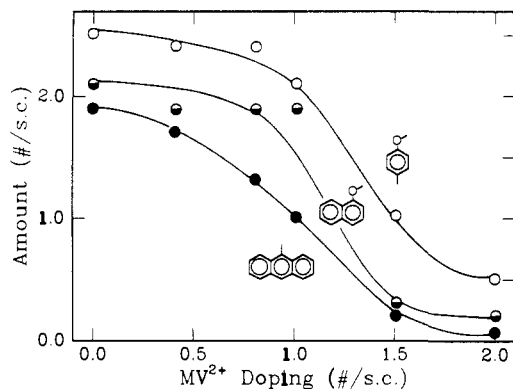


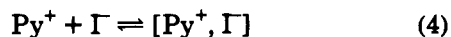
**Figure 7.** The synergistic effects of the donor size (shape) and the degree of  $MV^{2+}$  exchange in zeolite-Y for the intercalation of *p*-methoxytoluene (O),  $\alpha$ -methylnaphthalene (◐), and 9-methylanthracene (●) from hexane solution.<sup>15</sup>

selectivity via intracavity CT complexation was further supported by the amount of uptake of 9-methylanthracene into MV(2.0)Y (Y doped with two  $MV^{2+}$  ions per each supercage) being negligible with the concomitant absence of the corresponding CT coloration on the zeolite.

From the size distinction of the two closely related arenes pentamethyl- and hexamethylbenzene, which have kinetic diameters of 7.15 and 7.95 Å,<sup>18</sup> respectively, by the doped zeolite-Y in hexane slurry, it was suggested that a van der Waals width of roughly 8 Å is sufficient to inhibit an arene from complex formation with acceptors in the doped zeolites. Interestingly, however, hexamethylbenzene could be intercalated into the doped zeolite in the end, although at a substantially slower rate, either in the complete absence of hexane solvent or by increasing the temperature of the slurries to 80 °C in sealed tubes. The solvent-free intercalation of the relatively large donor was also accelerated by increasing the temperature of the mixture.<sup>19</sup> The eventual accommodation of hexamethylbenzene by the doped zeolite-Y, despite its equilibrium pore size (7.4 Å) being somewhat smaller than the kinetic diameter of the arene compound, was ascribed to the thermal vibration of both the zeolite framework and substrate.

## B. Stepwise Assembly of Pyridinium Iodide CT Salts

The pyridinium acceptors discussed in the previous section are also known to form a series of brilliantly colored salts with iodide.<sup>20–23</sup> Similarly, tropylium ( $TR^+$ ) forms an orange salt with iodide.<sup>23</sup> The bright colors arise from interionic electronic transitions involving charge transfer from the iodide donor to the organic acceptor, i.e.



The intracavity assembly of such highly colored CT salts in zeolite-Y was achieved by intercalating iodide salts from acetonitrile solution into various acceptor-doped zeolite-Y samples.<sup>24</sup> Since the overall size of an iodide salt is also determined by the size of its counteranion, the iodide salts with various counteranions were applied as the prototypical size probes for zeolite shape selectivity. Thus, when the doped zeolites were exposed to iodide salts of sodium, potassium, tetramethylammonium ( $TMA^+$ ), and tetraethylammo-

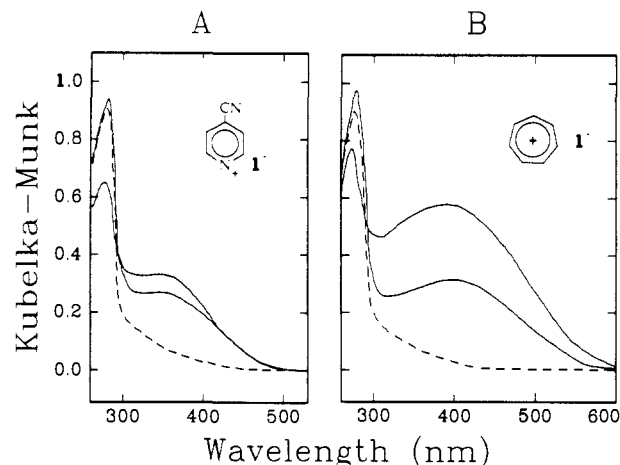


**Figure 8.** Diffuse reflectance spectra of the charge-transfer salts (A)  $PCP^+I^-$  and (B)  $TR^+I^-$  from the intercalation of 7 mM (bottom) and 0.3 M (upper) solutions of  $Na^+I^-$  in acetonitrile into zeolite-Y doped with  $PCP^+$  and  $TR^+$ , respectively. The dashed lines represent the corresponding spectra of untreated  $PCP(0.7)Y$  and  $TR(0.8)Y$  for comparison.<sup>24</sup>

onium ( $TEA^+$ ) dissolved in acetonitrile, dramatic colorations of the zeolites were noted immediately, while the supernatant solutions remained colorless. However, exposure to the iodide salts of the larger cations such as tetra-*n*-butylammonium ( $TBA^+$ ) and tetra-*n*-hexylammonium ( $THA^+$ ) led to no coloration.<sup>25</sup> In contrast, the iodide salts, regardless of the size of counteranions, immediately formed yellow to orange CT complexes in solution with the acceptor cations. Although ACY ( $AC^+$ -doped zeolite-Y) retained its yellow color when it was treated with iodide solutions of  $Na^+$ ,  $K^+$ ,  $TMA^+$ , and  $TBA^+$ , the characteristic green fluorescence of  $AC^+$  was immediately quenched, while such fluorescence quenching was not effected with iodide solutions of either  $TBA^+$  or  $THA^+$ , even after an extended period of exposure.

The sluggish or ineffective response of  $TBA^+$  and  $THA^+$  represents the steric restriction of the supercages of Y to the size of counteranion, since the kinetic diameter of  $TBA^+$  is  $\sim 8.1$  Å, which is above the upper limit for ready passage through the 7.4-Å aperture of Y. The strong dependence on the size of the counteranion also suggested that iodide penetration into the zeolite-Y supercage proceeded via ion-pair intercalation, especially via a contact ion pair, owing to the restricted space of the aperture and supercage of Y.

The brightly colored zeolites were spectroscopically characterized by comparison of their diffuse reflectance spectra with those of the corresponding crystalline charge-transfer salts with iodide. The diffuse reflectance spectra of the yellow and orange zeolites obtained from  $NaI$  and zeolite-Y doped with  $PCP^+$  and  $TR^+$  showing the well-resolved CT bands with  $\lambda_{max} = 360$  and 400 nm, respectively, are shown in Figure 8. The spectra also show the intensity of the CT bands of the colored zeolites to vary with an increase in iodide concentration in the makeup solution from 0.007 to 0.3 M, in accord with the following equilibrium:



within the supercages of Y. The iodide salts of the monocationic acceptors were slowly leached out of the

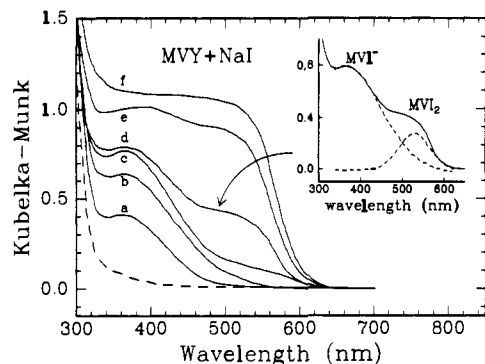
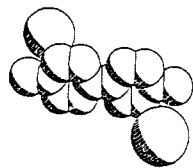


**Figure 9.** Stepwise formation of the ion pair  $MV^{2+}(I^-)$  and ion triplet  $MV^{2+}(I^-)_2$  identified by their charge-transfer spectra obtained from the intercalation of  $Na^+I^-$  from (a) 7, (b) 20, (c) 40, (d) 80, (e) 160, and (f) 320 mM solutions in acetonitrile. The dashed line is the diffuse reflectance spectrum of  $MV(1.0)Y$ . The inset shows the Gaussian deconvolution of the partially resolved CT envelope (d) into the ion pair and ion triplet components with  $\lambda_{max} = 362$  and  $528$  nm, respectively.<sup>24</sup>

zeolite cages into the supernatant solutions, indicating the reversible intercalation of iodide salts. The fact that the intensity of the CT envelope for zeolite-Y intercalating  $PCP^+I^-$  was lower than that of a  $TR^+I^-$  intercalate in Figure 8, obtained from the higher iodide concentrations, was ascribed to the more facile leaching of  $PCP^+I^-$  salt from the zeolite cages.

While the univalent cations  $PCP^+$  and  $TR^+$  did not show a color change with an increase of  $NaI$  concentration, as indicated by the invariance of  $\lambda_{max}$  in the diffuse reflectance spectra (Figure 8), the divalent cations  $MV^{2+}$  and  $DQ^{2+}$ , on the other hand, showed a marked difference in spectral features when doped zeolites were treated with  $NaI$  at different concentrations. The results are best illustrated by Figure 9. Thus at relatively low concentrations of  $NaI$  ( $<0.02$  M), a monotonic increase in the absorbance of a single, well-resolved band with  $\lambda_{max} = 362$  nm, was noted from  $MV^{2+}$ -doped Y, while the yellow persisted. At intermediate concentrations ( $\sim 0.08$  M), appearance of a new resolved band at  $528$  nm was apparent, while the color of zeolite gradually turned to orange. At the highest concentration of  $NaI$  examined ( $0.32$  M), the zeolite turned to brilliant red and the spectrum consisted of a single, broad, unresolved envelope that was reminiscent of that for crystalline  $MVI_2$  (bright red), whose structure is depicted by the space-filling perspective:



Coupled with the result of the intercalated amounts of  $NaI$  increasing with the increase of the concentration in the slurries (Figure 9), the yellow ( $\lambda_{max} = 362$  nm) and red ( $\lambda_{max} = 528$  nm) bands were ascribed to the contact ion pair (CIP)  $MV^{2+}(I^-)$  and ion triplet (CIT)  $MV^{2+}(I^-)_2$ , respectively. Accordingly, the spectral variations accompanying the changes in color of  $MV^{2+}$ -doped Y induced by different concentrations of  $NaI$

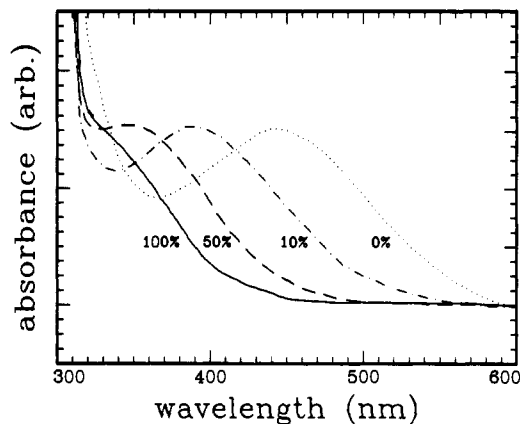
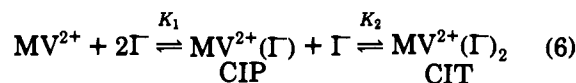


**Figure 10.** Solvatochromic shift of the charge-transfer band of methylviologen diiodide in aqueous acetonitrile containing 100%, 50%, 10%, and no water.<sup>24</sup>

were ascribed to multiple ionic equilibria which involved CIP and CIT, e.g.



Similar behavior was also observed from the analogous  $DQY$ . Such a clean distinction between the ion pairs and ion triplets is not possible in solution and therefore reflects the unique feature of zeolite cages. Unlike the univalent cationic salts of  $PCP^+$ ,  $TR^+$ , and  $AC^+$ , no leaching of the CT salts out of zeolite-Y cages was observed during the intercalation of  $NaI$ , since the ion pairs,  $MV^{2+}(I^-)$  and  $DQ^{2+}(I^-)$ , still retained overall positive charges and the ion triplets,  $MV^{2+}(I^-)_2$  and  $DQ^{2+}(I^-)_2$ , were not soluble in acetonitrile. Nevertheless,  $NaI$  could be readily removed by washing the colored zeolites with acetonitrile solvent. Thus, when the  $MV^{2+}(I^-)_2$ -containing zeolite-Y was washed with solvent, the red of the zeolite progressively turned to orange to yellow and finally to colorless, establishing the reversibility of the ionic equilibria.

The less soluble  $K^+I^-$  (in amounts corresponding to  $0.5$  M) was also readily intercalated into  $MVY$  and  $DQY$  as a slurry in acetonitrile to form initially the CIP and then the CIT within the supercages of zeolite-Y, accompanied by the complete dissolution of  $K^+I^-$ . Interestingly, however, iodide salts of  $TMA^+$  and  $TEA^+$  were effective only for the formation of CIP but not CIT, indicating the shape-selective modulation of the multiple ionic equilibria by the size of quaternary ammonium salts.

Since ionic CT salts have often been exploited as probes for solvent polarity,<sup>4,5</sup> the intracavity formation of ionic CT salts was also exploited to delineate the polarity of the zeolite-Y supercage. Thus as shown for the mono iodide complex of  $MV^{2+}$  in various solvent media of different degrees of polarity in Figure 10, the  $\lambda_{max}(CT)$  shifts to a lower energy region with the decrease of polarity of the medium. Such a solvatochromic shift of ionic CT salts originates from the decrease of the energy gap between the levels of the ground and excited states as the polarity of the medium decreases.<sup>5,23,26,27</sup> From the direct comparison of the yellow CT band of encapsulated  $MV^{2+}(I^-)$  ( $\lambda_{max} = 362$  nm) in zeolite-Y supercages in Figure 9 with those in Figure 10, the polarity of the zeolite-Y supercage was then estimated to be similar to that of 50% aqueous

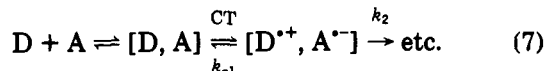
acetonitrile solvent. (A similar result was reached from an independent study as described in section III.B.1.)

In such polar solvents as water and aqueous acetonitrile, the diiodide salts  $MV^{2+}(I^-)_2$  and  $DQ^{2+}(I^-)_2$  are extensively dissociated since the individual ionic species are greatly stabilized by solvation. Thus a dilute aqueous solution of  $MV^{2+}(I^-)_2$  is usually colorless, and even after dissolution of excess NaI ( $\sim 1$  M), the solution only turns pale yellow, indicating a small association constant  $K_1$  for the formation of the ion pair. The second association constant  $K_2$  for triple-ion formation in water is even lower and approaches zero. In this regard, the singular behavior of the zeolite-Y supercage to allow formation of triple ions in the associated form, despite its polar nature, was interpreted in terms of the unique steric effects of zeolites. Such steric effects lead to many interesting results when a variety of organic and organometallic transformations are carried out within zeolites.

### III. Electron Transfer between Intercalated Molecules

#### A. Photoassisted Electron Transfer

The control of the ratio of the back electron transfer rate  $k_{-1}$  relative to the follow up reaction rate  $k_2$  during the charge-transfer activation of the precursor complexes [D,A] from donors and acceptors is critical for determination of the overall efficiency of the reaction,<sup>28</sup> i.e.



However, the available methodology for the general control of back electron transfer is limited.<sup>3,28</sup> In this regard, zeolites have been examined extensively to modulate the magnitude of back electron transfer rates during the photochemical activation of charge-transfer complexes<sup>29</sup> and sensitizer-acceptor systems.<sup>30-35</sup> All the results converged to a common experimental fact that, in zeolite cages, the back electron transfer rates are tremendously retarded relative to those in solution, presumably due to the unique steric and electrostatic effects of zeolite cages which can help stabilize the unstable transient species. The results are reminiscent of related work where the triplet excited states of carbonyl compounds entrapped within zeolites or adsorbed on polar supports showed highly prolonged lifetimes relative to those in solution.<sup>36-39</sup>

Photoexcitation of the CT bands of Ar-Py<sup>+</sup> complexes encapsulated within zeolite-Y with a 10-ns pulse from a Nd<sup>3+</sup>:YAG laser led to the simultaneous formation of transient CT ion pairs [D<sup>•+</sup>, A<sup>•-</sup>], which were detected by diffuse reflectance methods.<sup>29</sup> Thus, as shown in Figure 11A, the excitation of the Naph-MV<sup>2+</sup> complex at 355 nm<sup>40</sup> with a pulsed laser generated a transient spectrum, which was identified as the simple superposition of the spectral bands of MV<sup>•+</sup> and Naph<sup>•+</sup> existing as an ion pair as indicated by the dotted lines. When the encapsulated Ant-PCP<sup>+</sup> complex was excited at 532 nm, the production of the anthracene cation radical ( $\lambda_{\text{max}} = 725$  nm) accompanied the bleaching of the CT band ( $\lambda_{\text{max}} = 490$  nm). The transient absorptions decayed homogeneously over the entire envelope in a microsecond time scale.

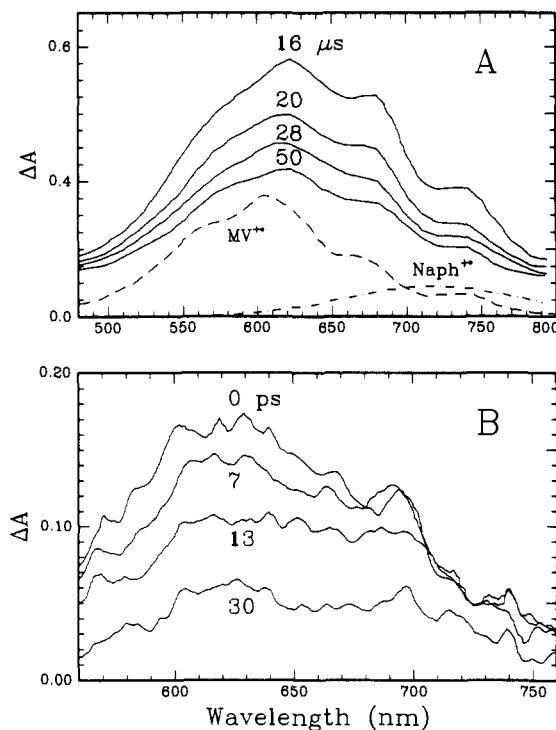


**Figure 11.** (A) Time-resolved diffuse reflectance spectra obtained at microsecond intervals following the 10-ns laser pulse at 355 nm of MV<sup>2+</sup>-naphthalene complex in zeolite-Y. The dashed lines represent the transient spectra of the radical ions MV<sup>•+</sup> and Naph<sup>•+</sup>. (B) Time-resolved picosecond absorption spectra following the 20 ps (fwhm) laser pulse at 355 nm of the same complex in acetonitrile solution.<sup>29</sup>

In strong contrast to the prolonged lifetimes of CT ion pairs produced within zeolite-Y supercages, the laser-flash photolysis of the same complexes generated in solution yielded spectral transients that could be detected only on the picosecond time scale, as compared in Figure 11B for the [MV<sup>•+</sup>, Naph<sup>•+</sup>] pair obtained from the excitation of the Naph-MV<sup>2+</sup> complex with a 20-ps pulsed laser in acetonitrile. The marked retardation of the back electron transfer rate of CT ion pairs in zeolite-Y was attributed to an adsorption effect of the ionic species on the polar aluminosilicate surface and stabilization by electrostatic fields. From the magnitude of the differences in Table V, the stabilizing effect of the zeolite-Y supercage on the CT ion pairs over that in solution was estimated to be  $\sim 8$  kcal mol<sup>-1</sup>.

An interesting photoelectron transfer between Ru(bpy)<sub>3</sub><sup>2+</sup> and MV<sup>2+</sup> molecules which were spatially separated in different supercages of Y was reported.<sup>30</sup> The intracavity synthesis of Ru(bpy)<sub>3</sub><sup>2+</sup> was carried out by heating Ru(NH<sub>3</sub>)<sub>3</sub><sup>2+</sup>-doped Y and 2,2'-bipyridine.<sup>31,41</sup> MV<sup>2+</sup> was introduced into the purified Ru(bpy)<sub>3</sub><sup>2+</sup>-doped Y by ion exchange, and the presence of the ionic species in the supercages of Y was confirmed by resonance Raman spectra in comparison with the corresponding spectra in solution. Since the diameter of Ru(bpy)<sub>3</sub><sup>2+</sup> was estimated to be  $\sim 13$  Å, the possibility of the presence of both ionic species within a 13 Å supercage was eliminated. The loading of Ru(bpy)<sub>3</sub><sup>2+</sup> was  $\sim 7\%$  of the total supercages and each of the rest of the supercages was doped with  $\sim 1$  MV<sup>2+</sup> ion.

Upon laser excitation of the thoroughly dehydrated and deoxygenated orange sample of Ru(bpy)<sub>3</sub><sup>2+</sup>-MV<sup>2+</sup>-Y at 413.1 (250 mW) or 457.9 nm (500 mW) for



**Table V. Spectral Decay of Charge-Transfer Ion Pairs in Zeolite-Y Supercage and in Acetonitrile Solution<sup>29</sup>**

Ar <sup>c</sup>	A <sup>+</sup> <sup>b</sup>	zeolite		acetonitrile	
		$\lambda_{CT}$ <sup>c</sup>	$\tau$ , <sup>d</sup> $\mu$ s	$\lambda_{CT}$ <sup>c</sup>	$\tau$ , <sup>d</sup> ps
Naph	MV <sup>2+</sup>	380	6.8	~360	30
	TR <sup>+</sup>	415	3.3	393	25
	OCP <sup>+</sup>	360 <sup>e</sup>	6.2	~330	
	PCP <sup>+</sup>	360 <sup>e</sup>	0.11	~330	25
Ant	MV <sup>2+</sup>	490	64	472	19
	TR <sup>+</sup>	520	4.2	488	25
	OCP <sup>+</sup>	449	9.2	425	
	PCP <sup>+</sup>	441	3.9	415	
9-MeAnt	MV <sup>2+</sup>	518	5.6	504	28
	PCP <sup>+</sup>	470 <sup>e</sup>		439	27
9,10-Me <sub>2</sub> Ant	MV <sup>2+</sup>			526	21
	PCP <sup>+</sup>			474	22

<sup>a</sup> Naph = naphthalene, Ant = anthracene, 9-MeAnt = 9-methylanthracene, 9,10-Me<sub>2</sub>Ant = 9,10-dimethylanthracene. <sup>b</sup> Acceptors. See text for abbreviation. <sup>c</sup> Charge-transfer band maximum (nm). <sup>d</sup> Lifetime as first-order decay. <sup>e</sup> From ref 19.

2–3 min, the color turned blue, which is characteristic of MV<sup>•+</sup>; the existence of the latter was also independently confirmed by resonance Raman spectra. However, the important evidence for the simultaneous formation of Ru(bpy)<sub>3</sub><sup>3+</sup> could not be obtained under the experimental conditions. Nonetheless, the process was ascribed to the photoelectron transfer from \*Ru(bpy)<sub>3</sub><sup>2+</sup> to MV<sup>2+</sup> in the nearby supercages. Although the time scale for the formation of an ion pair was not measured, the blue persisted for 1 h under anaerobic conditions and finally returned to orange, indicating the extremely slow thermal back electron transfer process from MV<sup>•+</sup> to Ru(bpy)<sub>3</sub><sup>3+</sup>. The rate of recovery of Ru(bpy)<sub>3</sub><sup>2+</sup> closely followed the decay of MV<sup>•+</sup>. The processes were attributed to the intercage electron transfer. However, it is more likely that the electron-transfer process occurs by the contact interactions of the ionic species through the interconnecting windows of 7.4 Å (vide supra), as the authors did not rule out this possibility.

The related electron-transfer quenching of the luminescence of Ru(bpy)<sub>3</sub><sup>2+</sup> by powerful electron donors such as *N,N,N',N'*-tetramethyl-1,4-phenylenediamine (TMPD, Wurster's reagent) and 10-phenylphenothiazine, which were spatially separated in different supercages of zeolite-X, was also examined.<sup>32</sup> Irradiation-induced formation of Ru(bpy)<sub>3</sub><sup>+</sup> and TMPD<sup>•+</sup> established a similar intercage photoelectron transfer but with \*Ru(bpy)<sub>3</sub><sup>2+</sup> acting as electron acceptor.

Dynamic electron-transfer quenching of the metal-to-ligand charge transfer (MLCT) excited state of Ru(bpy)<sub>3</sub><sup>2+</sup>, which was doped only onto the external surface of zeolite microcrystals (size excluded by 7–8-Å pore openings), by intrazeolitic MV<sup>2+</sup> ions revealed valuable information on the bimolecular quenching rate of \*Ru(bpy)<sub>3</sub><sup>2+</sup> by MV<sup>2+</sup> and diffusion coefficients of MV<sup>2+</sup> in zeolites.<sup>35</sup> The zeolites studied were Y, L, and mordenite.

When the deoxygenated, aqueous suspensions of the doped zeolites were irradiated at 532 nm by Nd:YAG Q-switched laser (11-ns pulses, 15–25 mJ per pulse), diffuse reflectance transient absorption spectra consist of two positive peaks at 400 and 600 nm (formation of MV<sup>•+</sup>) and a negative peak at 450 nm (bleaching of Ru(bpy)<sub>3</sub><sup>2+</sup> absorption). Lifetimes of transient signals varied depending on the types of zeolite and amount

**Table VI. Bimolecular Quenching Rate Constants of Ru(bpy)<sub>3</sub><sup>2+</sup> and MV<sup>2+</sup> and Diffusion Coefficients of MV<sup>2+</sup> in Zeolites L, Y, and Other Microenvironments<sup>a,35</sup>**

	$K_{sv}$ , M <sup>-1</sup>	$k_q$ , M <sup>-1</sup> s <sup>-1</sup>	$D_{MV^{2+}}$ , cm <sup>2</sup> s <sup>-1</sup>
zeolite-L	4.2	9.1 × 10 <sup>6</sup>	1.3 × 10 <sup>-7</sup> <sup>e</sup>
zeolite-Y	4.6 (1.8)	7.9 × 10 <sup>6</sup> (3.1 × 10 <sup>6</sup> )	7.9 × 10 <sup>-7</sup> <sup>e</sup> (4.4 × 10 <sup>-8</sup> )
hectorite <sup>b</sup>		1.1 × 10 <sup>6</sup>	
ZPS <sup>c</sup>	9.8	1.2 × 10 <sup>7</sup>	1.6 × 10 <sup>-8</sup>
aq soln <sup>d</sup>		5 × 10 <sup>8</sup>	

<sup>a</sup> Values in parentheses refer to powdered zeolite-Y samples air-dried in vacuo at 40 °C. <sup>b</sup> Reference 44. <sup>c</sup> Reference 45. <sup>d</sup> Reference 43. <sup>e</sup> Average pore radii of zeolites Y and L were taken to be 5 Å.

of loadings of Ru(bpy)<sub>3</sub><sup>2+</sup> and MV<sup>2+</sup>, but generally lasted more than 100 ms. Since there was interference from emission of \*Ru(bpy)<sub>3</sub><sup>2+</sup> at 600 nm the signals were monitored at 400 nm. The decay curves did not follow either first- or second-order kinetics, indicating a complicated recombination process between Ru(bpy)<sub>3</sub><sup>3+</sup> and MV<sup>•+</sup>. Interestingly, the recombination kinetics showed different dependences on the loading level of MV<sup>2+</sup> for zeolites L and Y, reflecting the different pore connecting pattern in the two zeolites. In both cases, the time scale for charge recombination was shorter than those observed in fully dehydrated zeolite-Y (vide supra).<sup>30,32</sup> In homogeneous solution, however, the bimolecular charge recombination follows equal concentration second-order kinetics.<sup>42,43</sup>

The time-resolved emission experiments also revealed that emission decays of \*Ru(bpy)<sub>3</sub><sup>2+</sup> do not follow single-exponential kinetics. However, in the absence of MV<sup>2+</sup> ions in zeolite pores, i.e., from the zeolite samples which adsorbed only Ru(bpy)<sub>3</sub><sup>2+</sup> on the outside of zeolite crystals, emission decays of \*Ru(bpy)<sub>3</sub><sup>2+</sup> follow single-exponential kinetics, indicating that any heterogeneity of adsorption sites available to Ru(bpy)<sub>3</sub><sup>2+</sup> on these zeolite surfaces is not reflected in the photophysics. Accordingly, the source of nonlinearity in the decay kinetics of \*Ru(bpy)<sub>3</sub><sup>2+</sup> in the Ru(bpy)<sub>3</sub><sup>2+</sup>- and MV<sup>2+</sup>-doped zeolite systems was attributed to the restricted diffusional motion of quencher MV<sup>2+</sup> in zeolite pores.

Linear Stern–Volmer plots were also derived from time-resolved emission and transient diffuse reflectance data for zeolites L and Y. Since the Stern–Volmer plots from both experiments were completely superimposable and show good linearity up to the maximum loading level (~1.5 M), the electron transfer quenching of \*Ru(bpy)<sub>3</sub><sup>2+</sup> by MV<sup>2+</sup> was concluded to be purely dynamic. Thus the quenching rate is controlled by diffusion of MV<sup>2+</sup> through zeolite pores. In the case of mordenite, which has relatively restricted channel systems (6.5 × 7.0 Å), nonlinear Stern–Volmer plots were observed. Table VI shows bimolecular quenching rate constants and diffusion coefficients of MV<sup>2+</sup> in zeolites L and Y obtained from steady-state emission, in comparison with other microenvironments.<sup>43–45</sup> The fact that quenching rate constants  $k_q$  in both zeolites are lower than those obtained in aqueous solutions<sup>46</sup> was rationalized in terms of more localized areas of contact between \*Ru(bpy)<sub>3</sub><sup>2+</sup> and MV<sup>2+</sup> and also in terms of restricted diffusion of MV<sup>2+</sup> through zeolite pores. The lower value of  $k_q$  in the partially dried zeolite-Y led the authors to conclude that the role of pore-filling water is important in enhancing the mobility of ions within zeolite pores.

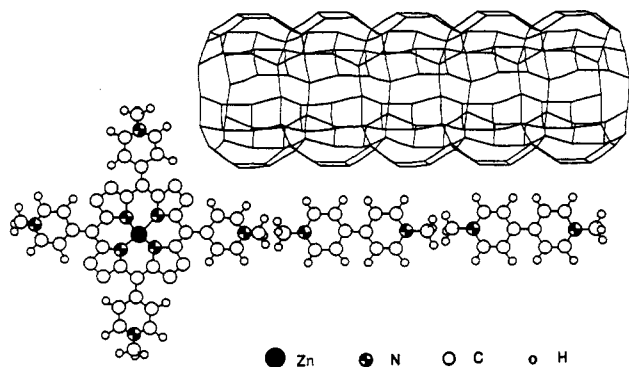


Figure 12. A perspective view of zeolite-L main channel and the ZnTMPyP<sup>4+</sup> and MV<sup>2+</sup> ions.<sup>33</sup>

The electron-transfer quenching of the singlet excited state of Zn<sup>II</sup>Por<sup>4+</sup> [Por<sup>2+</sup> = tetrakis(*N*-methyl-4-pyridyl)porphyrin] by MV<sup>2+</sup> exchanged in zeolite-L was exploited to generate hydrogen from water.<sup>33</sup> The bulky Zn<sup>II</sup>Por<sup>4+</sup> was size excluded and doped only onto the outside of zeolite-L crystals as a monolayer as represented in Figure 12. Singlet-state electron-transfer quenching was estimated to occur within a 10–100 ps time scale, at high loading of MV<sup>2+</sup>. For hydrogen evolution, the zeolite was intercalated with small aggregates of platinum (0.001–0.004 wt %) within the channels prior to doping with Zn<sup>II</sup>Por<sup>4+</sup> and MV<sup>2+</sup>. Hydrogen evolution was achieved by irradiating the zeolite in the visible region in aqueous solution containing ethylenediaminetetraacetic acid (EDTA) as the sacrificial electron donor. Since the related zinc-porphyrin with no *N*-methylpyridinium groups did not produce hydrogen, it was speculated that the electron-transfer quenching of <sup>1</sup>\*Zn<sup>II</sup>Por<sup>4+</sup> by MV<sup>2+</sup> occurred via contact interaction ( $\pi$ -overlap) between the *N*-methylpyridinium groups of the Por<sup>2+</sup> ligands sticking into the channels and MV<sup>2+</sup> induced by the close positioning of the two molecules at high loading of MV<sup>2+</sup>. The latter was supported by the fact that at low loading of MV<sup>2+</sup> (<0.4 MV<sup>2+</sup> per cage), where the  $\pi$ -overlap between the *N*-methylpyridinium and MV<sup>2+</sup> is likely to be avoided, no hydrogen evolution and singlet-state quenching were observed.

The back electron transfer rate was inferred to be extremely fast and efficient since the quantum yield of hydrogen evolution was only 0.003%. However, incomplete back electron transfer was inferred from the formation of MV<sup>•+</sup> after continuous irradiation of the nonplatinized zeolites for 10 h in the absence of EDTA. Interestingly, under the same experimental conditions, triplet-state quenching was not effective although the processes are exoergic in homogeneous solution and in micelles. This noneffective quenching was attributed to the shift of ground-state redox potentials of porphyrins adsorbed onto zeolite surfaces to more positive values by  $\sim 200$  mV.<sup>47</sup>

The construction of an interesting molecular triad in zeolite cages was also reported.<sup>34</sup> The triad consisted of Ru[(CH<sub>3</sub>)<sub>2</sub>bpy]<sub>3</sub><sup>2+</sup> and DQ<sup>2+</sup>, which were covalently linked by replacing one of the methyl groups of (CH<sub>3</sub>)<sub>2</sub>-bpy ligands of the Ru<sup>2+</sup> complex with an ethylene unit, one end of which is also connected at the 2 position of DQ<sup>2+</sup> as the portion of sensitizer-acceptor. The RuL<sub>3</sub><sup>2+</sup>-DQ<sup>2+</sup> was exchanged in roughly monolayer quantities onto the L or Y which was previously doped

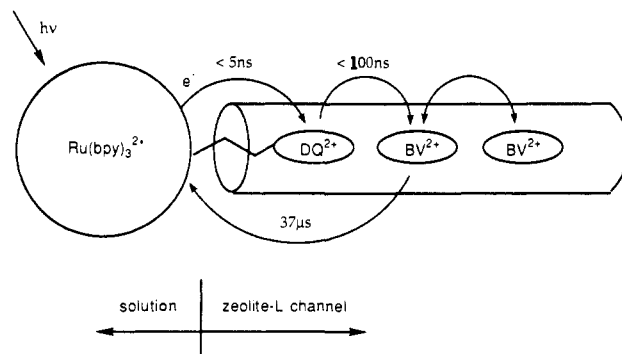


Figure 13. Possible spatial arrangement of the RuL<sub>3</sub><sup>2+</sup>-DQ<sup>2+</sup> and BV<sup>2+</sup> at the interface of zeolite-L and aqueous solution.<sup>34</sup>

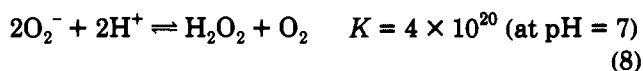
with benzylviologen (BV<sup>2+</sup>) as the secondary acceptor. Since the size of RuL<sub>3</sub><sup>2+</sup> is too big to be admitted into these zeolites, it was assumed that DQ<sup>2+</sup> of the complex ion was preferentially incorporated into the pores of zeolites according to the scheme illustrated in Figure 13.

The 10-ns pulsed laser excitation of zeolite samples in aqueous slurries at 532 nm showed a transient difference spectrum with absorption maxima at 400 and 600 nm and a minimum at 480 nm, which could be attributed respectively to the formation of BV<sup>•+</sup> and the bleaching of RuL<sub>3</sub><sup>2+</sup>. The formation of the Ru<sup>3+</sup>-BV<sup>•+</sup> charge-separated state occurred within 100 ns, which is the shortest time scale for such experimental conditions. Control experiments with Ru[(CH<sub>3</sub>)<sub>2</sub>-bpy]<sub>3</sub><sup>2+</sup> exchanged onto BV<sup>2+</sup>-doped L showed only modest quenching of the MLCT state by BV<sup>2+</sup>, indicating that the direct quenching of <sup>\*</sup>RuL<sub>3</sub><sup>2+</sup> by BV<sup>2+</sup> was unimportant. Accordingly, it was suggested that the Ru<sup>3+</sup>-BV<sup>•+</sup> charge-separated state occurred via intramolecular electron transfer from <sup>\*</sup>RuL<sub>3</sub><sup>2+</sup> to DQ<sup>2+</sup>, which proceeds within 5 ns in solution, followed by the subsequent electron transfer from DQ<sup>•+</sup> to BV<sup>2+</sup>. The quantum yield for the formation of the state was estimated to be  $\sim 17\%$ , and the state decayed via first-order exponential kinetics with a lifetime of  $\sim 37$   $\mu$ s. The rather prolonged lifetime of the Ru<sup>3+</sup>-BV<sup>•+</sup> was attributed to the spatial separation of the Ru<sup>3+</sup> and BV<sup>2+</sup>; however, the back electron transfer relayed by the DQ<sup>2+</sup> moiety could not be excluded.

## B. Thermal Electron Transfer

### 1. Superoxide Electron Transfer

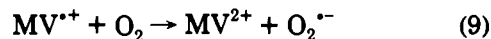
Superoxide O<sub>2</sub><sup>-</sup> is one of the most elusive species in solution due to its high reactivity with protons in protic solvents and its powerful nucleophilicity in aprotic solvents.<sup>48</sup> For example, in aqueous solution it decomposes rapidly into hydrogen peroxide and molecular oxygen according to the following equilibrium:



The equilibrium is obviously far to the right. Furthermore, superoxide is ESR silent in solution since the unpaired electron resides on the doubly degenerate  $\pi^*$  orbitals.<sup>49</sup> Furthermore, the colorless superoxide ion has only one characteristic electronic absorption in the region of 245–255 nm, where most other compounds usually have absorption, and the extinction coefficient of the band is relatively low ( $\epsilon = 1400$ –2500).

Accordingly, despite the importance of electron-transfer reactions involving superoxide formation in many reactions, the spectroscopic identification of the species has been rather unsatisfactory. In this regard, zeolites have been used to trap the elusive superoxide ions during many interesting reactions, since the molecular pockets of zeolites have a great potential to immobilize reactive species that are otherwise subject to rapid diffusive annihilation in solution. Furthermore, the superoxide ions trapped in zeolite cages can be easily identified by ESR spectroscopy since the double degeneracy of the  $\pi^*$  orbitals is removed when superoxide is adsorbed on the solid surface.<sup>49</sup>

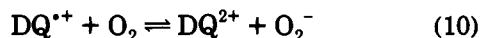
The reduction of molecular oxygen with cation radicals of methylviologen ( $MV^{•+}$ ) and diquat ( $DQ^{•+}$ ) has been widely accepted as a key step in many important reaction systems.<sup>20,48</sup> For example, the



herbicidal activity of the bipyridiniums and other related compounds has been ascribed to the involvement of the superoxide electron transfer with viologens.<sup>50,51</sup> However, evidence presented so far has been rather indirect.<sup>51,52</sup>

Direct evidence for the above reaction was established by deliberately performing the reaction within zeolite-Y supercages.<sup>53</sup> The  $MV^{•+}$ - and  $DQ^{•+}$ -doped zeolite-Y were prepared by slurring the dehydrated sodium zeolite-Y in acetonitrile solutions of  $MV^+PF_6^-$  and  $DQ^+PF_6^-$ , respectively. The resulting zeolites were brilliant blue ( $MV^{•+}$ ) and green ( $DQ^{•+}$ ), and the diffuse reflectance spectra of the highly colored samples revealed the characteristic absorption spectra of the ions, confirming the successful incorporation of the ions within the supercages (Figure 14). From the close similarity of the spectra in zeolites and in solution, it was inferred that the cation radicals exist as monomeric species within the supercages, since the spectra of the crystalline  $MV^+PF_6^-$  and  $DQ^+PF_6^-$  only showed featureless absorptions over the entire spectral range.

The ESR spectra of the doped zeolites showed isotropic signals with  $g$  values of 2.0030 ( $MV^{•+}$ ) and 2.0029 ( $DQ^{•+}$ ), respectively, in support of the monomeric nature of the encapsulated ions. The blue zeolite was bleached instantly at  $-78$  °C upon introduction of dioxygen, whereas the loss of the green color was slower under the same condition. The bleaching of the colors accompanied the disappearance of the isotropic signals with concomitant appearance of the typical ESR signals of superoxides in axial symmetry. The signals were stable below  $-20$  °C. The  $g$  values are listed in Table VII. Interestingly, the superoxide electron transfer with  $DQ^{•+}$  was reversible, i.e.



while the reaction with  $MV^{•+}$  was irreversible. Such a dramatic distinction between the cation radicals was attributed to the difference of the oxidation potentials of  $MV^+$  and  $DQ^+$ , with  $E^\circ = -0.45$  and  $-0.39$  V versus SCE, respectively. From this pair of reactions, the  $E^\circ$  of dioxygen was inferred to be close to  $-0.4$  V, since the reduction potentials of  $MV^{2+}$  and  $DQ^{2+}$  did not shift much in zeolite cages.<sup>47</sup> Furthermore, from the inferred reduction potential of dioxygen in Y, the polarity of

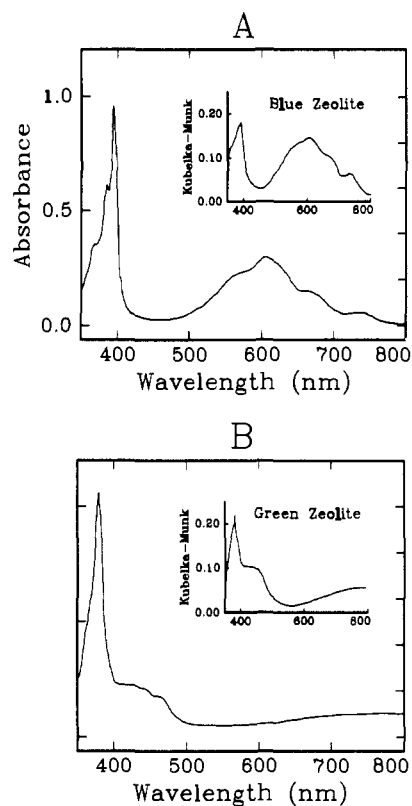
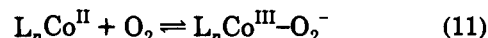


**Figure 14.** Comparison of the absorption spectra of (A)  $2.5 \times 10^{-5}$  M  $MV^+PF_6^-$  and (B)  $3.8 \times 10^{-5}$  M  $DQ^+PF_6^-$  in acetonitrile solution with the diffuse reflectance spectra of blue and green zeolites shown in the insets.<sup>53</sup>

the supercages was suggested to lie between water and DMF in comparison of the values in various solvents, since the  $E^\circ$  of dioxygen differed markedly, depending on the polarity of the medium.<sup>48</sup> Interestingly, similar polarity was suggested for zeolite-Y supercages from the independent experimental results of intrazeolite formation of CT salts<sup>24</sup> (vide supra).

Zeolites have also been effectively exploited to immobilize superoxo cobalt(III) complexes  $L_nCo^{III}-O_2^-$  ( $L$  denotes any nitrogen-, oxygen-, or carbon-based ligand such as amine, cyanide, water, and zeolite-framework oxygen, and the subscript  $n$  denotes an unspecified number of ligand; see Table VII) which otherwise rapidly transform into  $\mu$ -peroxo species in solution. The intracavity  $Co^{II}L_n$  complexes have been constructed in a stepwise manner by introducing the corresponding ligands into  $Co^{2+}$ -exchanged zeolites. The encapsulated  $Co^{II}L_n$  and the corresponding superoxo complexes, which were obtained by subsequently treating the complexes with molecular oxygen, were characterized usually by ESR spectroscopy.<sup>53-60</sup> The results are summarized in Table VII. In some cases,<sup>55-58</sup> even the formation of  $\mu$ -peroxo species was claimed. Since the  $Co^{II}L_n$  complexes bind molecular oxygen reversibly, i.e.



the  $Co^{II}L_n$  incorporating zeolites may be useful as oxygen carriers.

Other low-valent transition-metal ions such as  $Ti^{3+}$ ,  $Cr^{2+}$ , and  $Ni^+$  which were coordinated by zeolite surface oxygen have also been reported to form superoxo complexes.<sup>61-64</sup> Interestingly, in the case of  $Ti^{3+}$  ex-

Table VII. Summary of Superoxide Electron Transfer Reactions in Zeolites

zeolite	reductants	products	reversibility	ESR parameters						refs
				$g_z$	$g_y$	$g_x$	$a_z$	$a_y$	$a_x$	
Y	MV <sup>+</sup>	MV <sup>2+</sup> + O <sub>2</sub> <sup>-</sup>	no	2.084	2.005	2.005				53
Y	DQ <sup>+</sup>	DQ <sup>2+</sup> + O <sub>2</sub> <sup>-</sup>	yes	2.065	2.003	2.003				53
Y	Co <sup>II</sup> (Salen)	LCo <sup>III</sup> -O <sub>2</sub> <sup>-</sup>	yes	2.0780	2.0204		21	11.3		54
Y	Co <sup>II</sup> L <sub>n</sub>	[L <sub>n</sub> Co <sup>III</sup> -O <sub>2</sub> <sup>-</sup> ] <sup>2+</sup> <sup>a</sup> [L <sub>n</sub> Co <sup>III</sup> -O <sub>2</sub> -Co <sup>III</sup> L <sub>n</sub> ] <sup>5+</sup> <sup>c</sup>	yes	(2.804)	2.01	2.000	17.8	12.0	12.5) <sup>b</sup>	55, 56
Y	Co <sup>II</sup> (en) <sub>2</sub> <sup>2+</sup>	[(en) <sub>2</sub> Co <sup>III</sup> -O <sub>2</sub> <sup>-</sup> ] <sup>2+</sup> [(en) <sub>2</sub> Co <sup>III</sup> -O <sub>2</sub> -Co <sup>III</sup> (en) <sub>2</sub> ] <sup>5+</sup>	(yes) <sup>d</sup>	2.084	1.998	1.992	20	10	13	57, 58
Y	Co <sup>II</sup> (bpy)(tpy)	[LL'/Co <sup>III</sup> -O <sub>2</sub> <sup>-</sup> ] <sup>2+</sup>	yes	2.063	2.007	1.998	15.6	11.0	11.0	59
Y	Co <sup>II</sup> (CN) <sub>4</sub> <sup>2-</sup>	[L <sub>4</sub> Co <sup>III</sup> -O <sub>2</sub> <sup>-</sup> ] <sup>2-</sup>	yes	2.075	2.002		11.4	7.5		60
A, Y	Ti <sup>III</sup> L <sub>n</sub> <sup>e</sup>	[Ti <sup>IV</sup> -O <sub>2</sub> <sup>-</sup> ] <sup>3+</sup>	no	(2.0196)	2.0089	2.0031) <sup>f</sup>				61
				(2.0040)	2.017	2.003) <sup>g</sup>				62
Y	Cp <sub>2</sub> Cr <sup>h</sup>	[Cp <sub>2</sub> Cr] <sup>+</sup> , O <sub>2</sub> <sup>-</sup>	no							65
Y	Cr <sup>II</sup> L <sub>n</sub> <sup>e</sup>	[Cr <sup>III</sup> -O <sub>2</sub> <sup>-</sup> ] <sup>2+</sup>	yes	2.025	1.996	1.984				63
Y	Ni <sup>I</sup> L <sub>n</sub> <sup>e</sup>	[Ni <sup>II</sup> -O <sub>2</sub> <sup>-</sup> ] <sup>+</sup>								64
X	Na <sub>6</sub> <sup>5+</sup>	5Na <sup>+</sup> + Na <sup>+</sup> -O <sub>2</sub> <sup>-</sup>		2.116	2.005	1.999				49
A, X, Y	Na <sub>4</sub> <sup>3+</sup>	3Na <sup>+</sup> + Na <sup>+</sup> -O <sub>2</sub> <sup>-</sup>	(yes) <sup>i</sup>	(2.077)	2.077	2.002) <sup>f</sup>				49
				(2.113)	2.0066	2.0016) <sup>g</sup>				

<sup>a</sup> L = NH<sub>3</sub>, NH<sub>2</sub>CH<sub>3</sub>, NH<sub>2</sub>Pr. <sup>b</sup> L = NH<sub>3</sub>. <sup>c</sup> L = NH<sub>3</sub>, NH<sub>2</sub>CH<sub>3</sub>. <sup>d</sup> Partially. <sup>e</sup> L = zeolite surface. <sup>f</sup> Zeolite-Y. <sup>g</sup> Zeolite-A. <sup>h</sup> Cp = cyclopentadienyl, C<sub>5</sub>H<sub>5</sub>. <sup>i</sup> O<sub>2</sub> was desorbed at 500 °C.

changed in zeolite-A, the formation of Ti<sup>IV</sup>-O<sub>2</sub><sup>-</sup> was only induced by visible irradiation,<sup>62</sup> whereas the formation of the same species in zeolite-Y occurs instantaneously at ambient temperatures. The trapped electron which is stabilized in the form of ionic sodium cluster Na<sub>4</sub><sup>3+</sup> or Na<sub>6</sub><sup>5+</sup> (discussed in detail in section IV.A) located within the repeating sodalite unit of zeolites A, X, Y, and sodalite, also forms zeolite-encapsulated sodium superoxide Na<sup>+</sup>O<sub>2</sub><sup>-</sup> upon oxygen treatment.<sup>49</sup> Zeolite-encapsulated chromocene Cp<sub>2</sub>Cr (Cp = cyclopentadienyl, C<sub>5</sub>H<sub>5</sub>) was smoothly oxidized by molecular oxygen to result in the formation of chromicinium Cp<sub>2</sub>Cr<sup>+</sup> and superoxide O<sub>2</sub><sup>-</sup>.<sup>65</sup>

### 2. Oxidation of Organic Compounds with Metal Ions

Transition metal ions such as Cu<sup>2+</sup> and Fe<sup>3+</sup> that were ion exchanged into zeolites have been shown to effectively oxidize arenes such as benzene, naphthalene, anthracene, pyrene, and perylene.<sup>66,67</sup> Furan and its methyl-substituted derivatives were also readily oxidized by Cu<sup>2+</sup> to result in the formation of the corresponding arene cation radicals and Cu<sup>+</sup>.<sup>68</sup> Formation of the latter was unambiguously established by X-ray photoelectron spectroscopy. The decrease of Cu<sup>2+</sup> signal intensity upon adsorption of 1-butene was attributed to the reduction of Cu<sup>2+</sup> by the olefin.<sup>69</sup> The transition-metal ions also effectively served as oxidative coupling agents during the polymerization of thiophene<sup>70</sup> or pyrrole<sup>71</sup> monomer within the interiors of zeolites. The polymerization reactions are summarized in more detail in section IV.A.

### 3. Redox Reactions between Inorganic Compounds

Oxidation of transition-metal ions with molecular oxygen O<sub>2</sub> has been widely applied to achieve higher oxidation states of the metal ions in zeolites.<sup>7</sup> NO<sub>2</sub> was also applied to oxidize Cu<sup>+</sup> to yield Cu<sup>2+</sup> and NO<sub>2</sub><sup>-</sup>.<sup>8a</sup> Oxidation of zeolite-encapsulated metallocenes Cp<sub>2</sub>M (M = Fe, Co, and Cr) with O<sub>2</sub> led to the formation of the corresponding metallociniums Cp<sub>2</sub>M<sup>+</sup>.<sup>65</sup> Especially in the case of the latter, simultaneous formation of superoxide ion O<sub>2</sub><sup>-</sup> was observed. Formation of an interesting complex [(en)<sub>2</sub>Ni-Cl<sub>2</sub>]<sup>2+</sup> (en = ethylenediamine) encapsulated within zeolite-Y supercages was achieved by treating Ni(en)<sub>2</sub><sup>2+</sup> with Cl<sub>2</sub> at low temperature.<sup>72</sup>

Hydrogen gas has been extensively applied as a reducing agent in the formation of metal ions in unusually low oxidation states and even to aggregated metal ions.<sup>7</sup> Carbon monoxide CO has also been widely applied as a mild reducing agent for the reduction of Cu<sup>2+</sup>, Ni<sup>2+</sup>, and Ag<sup>+</sup>.<sup>7,73</sup> Redox reaction between NO and the transition-metal ions such as Cu<sup>2+</sup>, Ni<sup>2+</sup>, Fe<sup>2+</sup>, and Cr<sup>2+</sup> leads to the formation of nitrosonium ion NO<sup>+</sup>, and monovalent metal ions.<sup>8a,74-76</sup>

Direct evaporation of metals onto zeolites also effects reduction of exchanged metal ions.<sup>77</sup> Usually, low-boiling metals with relatively low ionization potentials have been chosen for such processes. Thus when sodium was evaporated onto Ni<sup>2+</sup>-doped zeolites, formation of Ni<sup>+</sup> species resulted. Similarly, mercury vapor deposition effected the transformations of Ag<sup>+</sup> to aggregated silver and Hg<sup>2+</sup> to Hg<sub>2</sub><sup>2+</sup>.

## IV. Zeolite Framework as Electron Donor and Acceptor

Zeolite frameworks which consist of silicon and aluminum oxide have behaved as more than merely innocent compartments for intercalated molecules. Rather, they have extensively participated as both electron donors and acceptors toward a variety of substrates in many important reactions. Such amphoteric properties of zeolites have often been shown to be largely dependent on the framework structure, nature of pretreatment, type, and number of exchanged cations, and silicon to aluminum ratio. As a result, zeolites have been employed as versatile media for many useful and interesting organic and inorganic transformations.

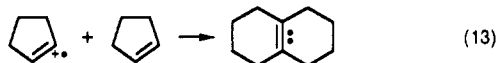
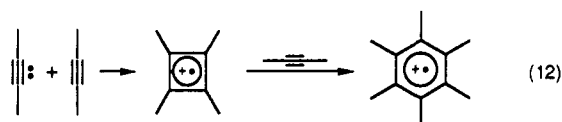
### A. Zeolite Framework as Electron Acceptor

#### 1. Induction by Thermal Treatment

It has long been known that the mere exposure of organic molecules such as diphenylethylene, triphenylamine, quinoline, and perylene, which have relatively low ionization potentials, onto thermally activated zeolite-Y at ambient temperature, leads to the formation of cation radicals.<sup>78,79</sup> The compounds whose ionization potentials are much higher than the polynuclear aromatic compounds, such as pentene-1, benzene,

methyl-substituted benzenes, and aniline, have also been shown to be readily oxidized by those zeolites in which  $H^+$ ,  $Ca^{2+}$ , or rare-earth cations were exchanged.<sup>78,80,81</sup> Formation of a benzene dimer cation<sup>82–85</sup> and subsequent transformation into a biphenyl cation radical<sup>85</sup> upon adsorption of benzene to  $H^+$ -exchanged mordenite (HM) have been demonstrated.  $H^+$ -exchanged ZSM-5 (HZSM-5) also showed similar electron-accepting properties toward adsorbed benzene.<sup>86,87</sup> The reversible formation of a benzene dimer cation radical in HZSM-5 was demonstrated in a recent report<sup>88</sup> by showing the disappearance of the ESR signal of the cation upon evacuation of the benzene-adsorbed zeolite.

Cation radicals of alkenes and alkynes generated in zeolites often have a tendency to rearrange into more stable cation radicals. Thus, when 3,3-dimethyl-1-butene  $CH_3C(CH_3)_2CHCH_2$  was adsorbed on thermally activated HZSM-5 at 123 K, a more stable cation radical of 2,3-dimethyl-2-butene  $C(CH_3)_2C(CH_3)_2$  was observed.<sup>89</sup> Similarly, a hexamethylbenzene cation radical was produced upon adsorption of dimethyl acetylene onto HZSM-5, presumably via aromatization of the alkyne cation radical with two additional neutral substrates.<sup>89</sup> This reaction was reinvestigated using HM as the oxidant in a recent report<sup>90</sup> in which the transformation of dimethylacetylene into hexamethylbenzene cation radical was claimed to proceed via a tetramethylcyclobutadiene cation radical intermediate (eq 12). Generation of cyclopentene cation radical and subsequent transformation into that of 9-octalin in HM was also proposed (eq 13).<sup>90</sup>



Deprotonation of cation radicals has been an alternative type of follow-up reaction to produce neutral radicals in zeolites. Thus, adsorption of ethylbenzene onto HZSM-5 or HM led to the formation of neutral radicals at the  $\alpha$ - or  $\beta$ -position of the ethyl substituent.<sup>91</sup> This reaction is more likely to proceed via oxidation of the alkylbenzenes followed by subsequent deprotonation of the cation radicals by zeolite-framework oxygens. Formation of a biphenyl cation radical from benzene cation radicals<sup>85</sup> is also possible only when the benzene cation radicals deprotonate. Similarly, transformation of a cyclopentene cation radical  $C_5H_5^+$  into a neutral allylic radical via deprotonation was proposed.<sup>92</sup> However, this reaction was recently reinvestigated and it was concluded that the initially generated paramagnetic species at 77 K must be a cation radical of 9-octalin.<sup>90</sup>

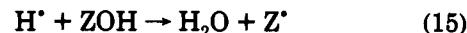
The formation of coke deposits over zeolite catalysts in many reactions may also be related to the complex follow-up reactions of cation radicals, especially at relatively high reaction temperatures. Indeed, various paramagnetic species were observed from the coke deposits which were generated by passing ethylene or propylene over HM.<sup>93,94</sup> The ESR signals of the resulting coke deposits were significantly different at different reaction temperatures. The careful analyses of the ESR signals led to a suggestion that the "high-

temperature coke" (>500 K) represents polyaromatic cation radicals and the "low-temperature coke" (380–470 K) olefinic or allylic radicals of oligomeric olefins. The radicals were stable over a period of months.

Metallocenes such as  $Cp_2Fe$ ,  $Cp_2Co$ , and  $Cp_2Cr$  have also been demonstrated to be easily oxidized by zeolites.<sup>65,95</sup> Oxidation of such organometallic compounds were especially effective when the compounds were evaporated onto  $H^+$ -exchanged zeolite-Y (HY). Oxidation of ferrocene also occurred in NaY but to a lesser extent. Oxidation of the other metallocenes  $Cp_2M$  ( $M = Co$  and  $Cr$ ) in NaY required the deliberate addition of oxidant  $O_2$ . The authors proposed that the oxidation of ferrocene in protic zeolites proceeds via an initial redox reaction between ferrocene and a proton to give a ferricinium ion and a hydrogen atom (eq 14),

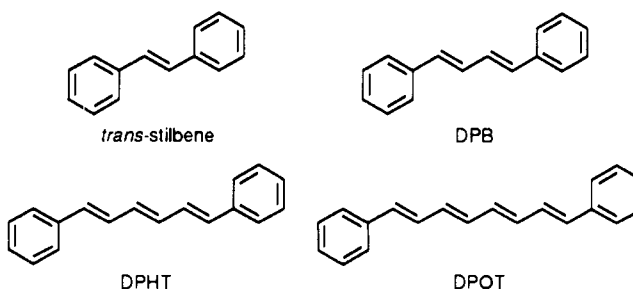


followed by subsequent dehydroxylation of a zeolite hydroxyl group ZOH (Z denotes framework silicon or aluminum) by hydrogen atom to result in the formation of a trivalent silicon or aluminum atom and a water molecule (eq 15), i.e.



Such a mechanism was based on the observation that the framework O–H stretching bands from zeolite-Y supercages ( $\alpha$ -cages) disappeared with the simultaneous growth of the characteristic infrared bands due to O–H stretching of water when the adsorption of ferrocene was monitored by in situ IR spectroscopy. The  $Al^+$  and  $Si^+$  radicals centered in zeolite lattice were detected by ESR spectroscopy. The presence of the blue ferricinium ions within zeolites was confirmed by diffuse reflectance UV–vis, IR, ESR, and Mössbauer spectroscopy.<sup>95</sup>

The remarkable properties of zeolites for generating and stabilizing the entrapped organic cation radicals have enabled zeolites to be used as novel media for the determination of steady-state fluorescence spectra of some interesting polyene cation radicals.<sup>96</sup> Thus, when *all-trans*- $\alpha,\omega$ -diphenyl polyenes such as *trans*-stilbene, 1,4-diphenyl-1,3-butadiene (DPB), 1,6-diphenyl-1,3,5-hexatriene (DPHT), and 1,8-diphenyl-1,3,5,7-octatetraene (DPOT) were adsorbed onto NaZSM-5 (thermally activated at 500 °C for 12 h) in nonpolar solvent at ambient temperature, a rapid coloration of the zeolite powders resulted, while the supernatant solutions remained colorless.



The fact that zeolite coloration arises from intrazeolite formation of cation radicals from the adsorbed  $\alpha,\omega$ -diphenyl polyenes was verified by the excellent matching of the diffuse reflectance spectra of the highly colored zeolite samples with those of the corresponding

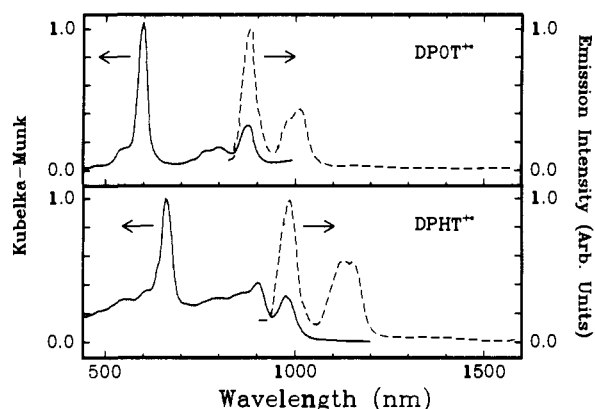
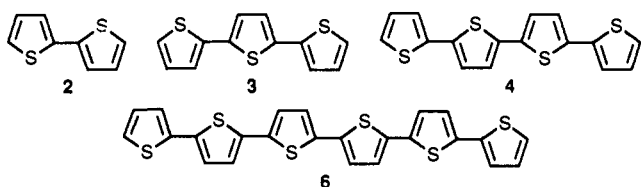


**Figure 15.** Emission (77 K) and diffuse reflectance (room temperature) spectra of DPHT<sup>2+</sup> and DPOT<sup>2+</sup> (as indicated) included in NaZSM-5.<sup>96</sup>

polyene cation radicals prepared by pulse radiolysis,<sup>97</sup> and by ESR studies. While in general organic cation radicals are vulnerable to nucleophilic attack,  $\alpha,\omega$ -diphenyl polyene cation radicals entrapped in NaZSM-5 were found to be indefinitely stable even when refluxed in methanol and water. The result was contrasted with their short lifetimes in solution ( $\mu$ s) and in solid matrices (s).<sup>98</sup> The remarkable stability of these cation radicals in ZSM-5 was attributed to the tight fit of the rod-shaped molecules in the narrow channels, since the cation radicals generated in a larger pore zeolite Na- $\beta$ , which possesses two sets of perpendicular channels with dimensions significantly larger than those in ZSM-5 (one circular with 5.6-Å diameter and one elliptical with dimensions  $6.0 \times 7.3$  Å), were unstable. The redox potential of NaZSM-5 was estimated to be close to 1.6 eV (vs SCE) from the fact that *trans*-4-carbomethoxystilbene ( $E^\circ_{\text{ox}} = 1.65$  V vs SCE) was not oxidized while the related *trans*-4-substituted-stilbenes with methoxy, dimethylamino, methyl, and chloro as the substituents ( $E^\circ_{\text{ox}} < 1.6$  V vs SCE) were all readily oxidized under the same condition.

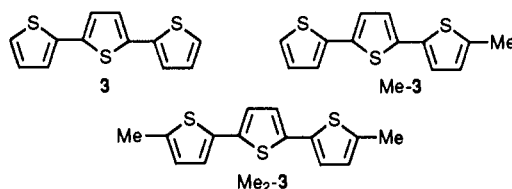
Most interestingly, DPHT<sup>2+</sup> and DPOT<sup>2+</sup> intercalated within NaZSM-5 gave emission spectra at excitation wavelengths between 350 and 850 nm at both 77 K and room temperature as shown in Figure 15. The emission spectra of the cation radicals were suggested to originate from the lowest spin-allowed excited states of the cation radicals based on the close coincidence of the absorption and emission peaks and their mirror symmetry. The absence of heavy atom effects on either the peak positions or the emission intensities upon changing the zeolite counteraction from Na<sup>+</sup> to Tl<sup>+</sup> further supported the spin-allowed doublet-doublet nature of the transitions.

Zeolites were also elegantly utilized to delineate the evolution of the electronic structure of organic conducting polymers with chain length.<sup>99</sup> Thus when the preformed neutral thiophene oligomers with chain lengths of two, three, four, and six, i.e.

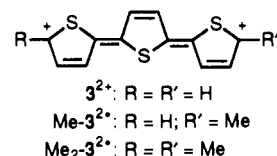


were included in thermally activated NaZSM-5 or Na- $\beta$  using trimethylpentane as solvent, immediate oxidation (cationic doping) of the oligomers within the interiors of zeolite pores occurred and further oxidative oligomerization among the included precursor oligomers slowly followed. Formation of the cation radicals (polarons) of the precursor oligomers was characterized by careful analyses of the ESR and diffuse reflectance UV-vis-NIR spectra of the oligomers included in the zeolites. As a typical example, the Na- $\beta$  which included terthiophene (deep red-purple) yielded a diffuse reflectance spectrum which consists of a peak due to absorption of the neutral precursor (354 nm, pale yellow) and a new peak (522 nm) in the visible region due to terthiophene cation radical  $3^{2+}$ , which agrees well with the transient spectrum of the cation radical generated by flash photolysis in solution. The highly colored zeolite sample also gave a strong ESR spectrum with a poorly resolved hyperfine structure verifying the generation of cation radicals. The peak positions of the cation radicals in the diffuse reflectance spectra shifted to red with increasing chain lengths of the precursor oligomers.

The cation radical of terthiophene is stable but upon standing or with mild heating (60–140 °C) new bands appeared at longer wavelength region due to further oligomerized products such as hexamers and nonamers. As one might expect, the resulting higher oligomers produced within the zeolite channels were assumed to be linear and well isolated from other strands of oligomers since the channel dimensions of the zeolites (5–7 Å) would not allow oligomerization at the  $\beta$ -position or  $\pi$ -overlap of any two strands within a single channel. Furthermore, the chain lengths of the oligomers could also be controlled by blocking the  $\alpha$ -positions of the precursor oligomers as demonstrated by the following methylated terthiophene derivatives, i.e.



Thus the diffuse reflectance spectra of these compounds included in ZSM-5 showed the corresponding absorption peaks due to cation radicals (polarons) in the region near 530 nm with a systematic bathochromic shift with increasing methyl substitution. At later reaction times, all three samples showed a sharp slightly structured band between 800 and 900 nm with the band shifting to longer wavelength by 300  $\text{cm}^{-1}$  per methyl substitution as shown in Figure 16. A careful analysis of the spectra led to the reasonable conclusion that the new peaks are due to dications (bipolarons), i.e.



In addition, the small well-resolved peaks at longer wavelengths (1000–1100 nm) for 3 and Me-3 were

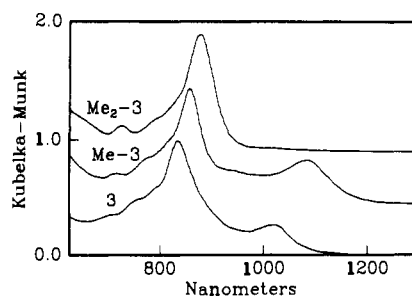


**Figure 16.** Diffuse reflectance of 3, Me-3, and Me<sub>2</sub>-3 included in NaZSM-5 in the region between 625 and 1300 nm. The spectra were normalized to unit absorbance and displaced vertically for clarity.<sup>99</sup>

**Table VIII. Electronic Absorption Band Positions for Oligomeric Thiophenes (2 ≤ n ≤ 9) Included in Na-ZSM-5.<sup>99</sup>**

chain length	neutral	polaron	bipolaron	bipolaron
2	300	407		
3	354	522		833
4	390	614	636	1046
6	434	775	600	1019
8			661	1383
9			761	1450

<sup>a</sup> The positions cited are the peak maxima in nanometers for the O–O vibronic transitions observed in room-temperature diffuse reflectance spectra. Higher energy vibronic peaks are not included.

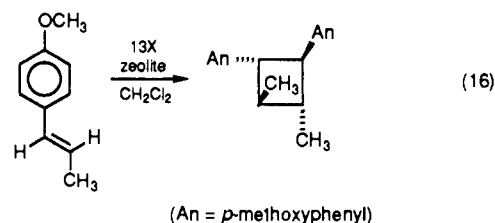
assigned to be absorptions of the dications (bipolarons) of the hexamers and dimethyl hexamers, since the red-shift of 550 cm<sup>-1</sup> per methyl group is roughly twice the effect observed for the methyl derivatives of 3<sup>2+</sup> and such a peak was singularly absent for the dimethyl derivative.

Further systematic experiments with other thiophene oligomers enabled the authors to derive the important electronic absorption bands of the cation radicals (polarons) and dications (bipolarons) of the oligomeric thiophenes (Table VIII). Extrapolation of this data led eventually to the delineation of the evolution of the electronic structure of conducting thiophene polymers. Such elegant work underscores the remarkable properties of zeolites of stabilizing entrapped reactive species that are otherwise doomed to rapid annihilation in conventional media.

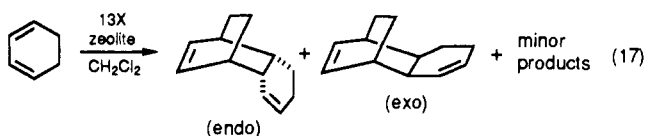
Similar polymerization of thiophene<sup>70</sup> and pyrrole<sup>71</sup> within the interiors of zeolite-Y and mordenite has also been achieved by employing the corresponding monomer as the precursor. However, ion exchange of transition-metal ions such as Cu<sup>2+</sup> and Fe<sup>3+</sup>, which are relatively strong oxidants, into zeolites was prerequisite to perform the polymerizations since these monomers require a much higher oxidizing potential than the pure zeolite-based oxidation sites (transition metal ion free) can offer.<sup>96</sup> The exact role of the exchanged transition metal ions during the polymerization reaction was not specified, but it is likely that oxidation of the monomers is involved.<sup>68</sup> Similarly, polymerization of aniline monomer within proton-exchanged zeolite-Y (HY) and mordenite (HM) could be only accomplished by deliberately adding a strong oxidant (NH<sub>4</sub>)<sub>2</sub>S<sub>2</sub>O<sub>8</sub> to the anilinium C<sub>6</sub>H<sub>5</sub>NH<sub>3</sub><sup>+</sup>-doped zeolites.<sup>100</sup> Polymerization of acetylene on the surface of thermally treated K<sup>+</sup>-exchanged zeolite-X (KX)<sup>101</sup> and transition metal ion (Co<sup>2+</sup>, Ni<sup>2+</sup>) exchanged zeolites (A, Y, ZSM-5)<sup>102</sup> was

also reported. In the latter case, it was implied that the charge-transfer interaction of acetylene with Co<sup>2+</sup> and the participation of framework Lewis acid sites are important during the polymerization reaction.

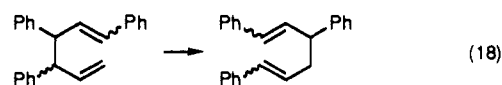
The use of zeolites as practical hole catalysts has been demonstrated by applying them in pericyclic reactions such as olefin cycloaddition, Diels–Alder reactions and Cope rearrangements.<sup>103–105</sup> Thus when 50–60 mg of *trans*-anethole (4-propenylanisole) was stirred with 2–3 g of NaX (Na<sup>+</sup>-exchanged zeolite-X, often called 13X) suspended in dichloromethane (5–7 mL) under reflux for 48 h, about 25% yield of the [2 + 2] cycloaddition product, *trans,anti,trans*-cyclobutane dimer, was obtained (eq 16).



NaX also catalyzed the Diels–Alder cycloaddition of 1,3-cyclohexadiene under similar conditions (eq 17). The observed yield was 13% with an endo/exo ratio of 3.8, after refluxing in dichloromethane for 24 h.



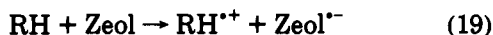
Since uncatalyzed thermal Diels–Alder dimerization of 1,3-cyclohexadiene resulted in only a 30% yield after heating at 200–250 °C for a period of 2 days and the well-known, highly active hole catalysts *tris*(*p*-bromophenyl)aminium salts<sup>105</sup> and cation radical polymer effected the dimerization of the cyclohexadiene in a 70% yield within 5 min at 0 °C, it was suggested that NaX acted as a mild hole catalyst in the above two reactions. The zeolite catalyses were even more effective when the slurried reaction mixtures were irradiated by a medium-pressure mercury lamp using a Pyrex filter. Indeed, conversion of 1,3-cyclohexadiene by Diels–Alder type reaction increased to 37% after irradiating for only 5 h. Similarly, [2 + 2] cycloaddition of the less electropositive  $\beta$ -methylstyrene, which was ineffective without irradiation, also produced a small amount of cycloaddition product with the aid of photostimulation. Such photoassisted zeolite catalyses were especially effective for Cope rearrangement of the racemic mixture (erythro and threo) of 1,3,4-triphenyl-1,5-hexadiene to give the 1,3,6-triphenyl-isomer in 54% yield after 40.5 h (eq 18). Surprisingly, the attempted



hole catalysis of this rearrangement using *tris*(*p*-bromophenyl)aminium salts and photosensitization with *p*-dicyanobenzene all failed. Cope rearrangement of *meso*- or *dl*-3,4-diphenyl-1,5-hexadiene was ineffective under the given conditions since the compound lacked a chromophore which absorbs Pyrex-filtered light.

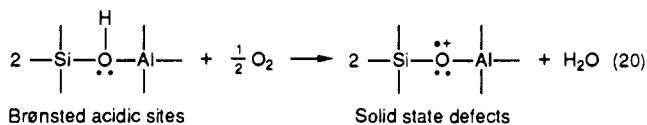
Accordingly, the highly enhanced activity of the zeolite catalyses by photoirradiation in the above reactions was ascribed to electron transfer from the excited states (presumably triplet) of organic substrates to NaX framework.

As has been presented in the above examples, the formation of organic and organometallic radicals on thermally treated zeolites is well documented. The formation of various cation radicals over zeolites from the corresponding substrates (RH) can be generalized as an electron-transfer reaction from the substrates to zeolites, i.e.



where "Zeol" denotes the zeolite framework.

Although the electron-accepting property of zeolites has long been established, the whereabouts of trapped electrons within the zeolite framework has been an interesting subject of debate. It has been suggested that metal impurities such as  $\text{Fe}^{3+}$  could function as oxidants.<sup>79,93</sup> Involvement of either Brønsted<sup>95</sup> or Lewis<sup>93,94</sup> acidic sites was also postulated. The solid-state defects which are positive holes on oxygen atoms of zeolite frameworks, generated by thermal activation under flow of oxygen or air (eq 20), have been claimed

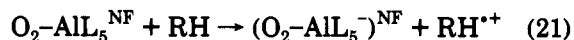


to be responsible for the remarkable oxidizing power of zeolites. Thus the ready oxidation of ethylene with an ionization potential (IP) of 10.50 eV, methanol with IP = 10.85 eV, and even acetylene with IP = 11.41 eV by zeolites was rationalized in terms of the high energy required to generate such localized solid-state defects which are roughly comparable with the ionization potential of the nonbonding electron pair of a water molecule (12.61 eV).<sup>81</sup>

The molecular oxygen which is strongly chemisorbed on zeolite frameworks while calcining zeolites under air or oxygen atmosphere has also been suggested to be a genuine electron acceptor.<sup>79,83,100</sup> In relation to this, enhancement of ESR signals of benzene cation radicals induced by adsorption of  $\text{O}_2$  or  $\text{SO}_2$  onto HM was observed.<sup>84</sup> It was suggested that the coordinatively unsaturated framework aluminum atoms (three-coordinated), which are generated by the loss of framework oxygen during thermal treatment, are responsible for the formation of benzene dimer cations. Hence the adsorption of oxygen or sulfur dioxide onto the three-coordinated aluminum atoms results in a positive shift of the redox potential of Al sites. In contrast, the nonframework, positively charged aluminum oxide  $\text{Al}(\text{OH})_2^+$  which is lost from the framework during activation has also been suggested to be the electron acceptor.<sup>107</sup> In a recent report,<sup>81</sup> the effect of oxygen on increasing the oxidizing power of Al sites was reinvestigated, and the study led to the conclusion that the nonframework aluminum species, especially those which are coordinatively distorted or unsaturated, rather than framework aluminum sites, are important in the formation of aniline cation radicals on HM and HY. Thus when aniline was adsorbed on HM which

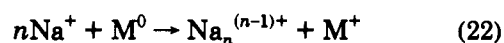
was treated with oxygen and evacuated at 550 °C prior to exposure to the substrate at ambient temperature, a strong ESR signal of the aniline cation radical arose immediately. When a small amount of molecular oxygen was introduced into the system, a new ESR signal arose which was analyzed to be a composite spectrum of superoxide ion  $\text{O}_2^-$  and the initial aniline cation radical but with somewhat increased intensity (by a factor of 1.3). The sextet superhyperfine structure of the  $g_{zz}$  component of  $\text{O}_2^-$  indicated that the superoxide ion was in weak interaction with an aluminum nucleus ( $I = 5/2$ ).

In contrast, when aniline was adsorbed on an HY sample which was similarly pretreated, only a very weak signal was yielded after 48 h. A dramatic increase of the ESR signal due to aniline cation radical and the concomitant rise of superoxide signal occurred upon introduction of oxygen (~120 Torr). The solid-state  $^{27}\text{Al}$  MAS NMR spectra of the HY sample after pretreatment revealed the appearance of a new signal at about 33 ppm which was assigned to the pentacoordinated nonframework aluminum species  $\text{AlL}_5^{\text{NF}}$  (L = nonspecific oxygen ligand). In the case of HM, however, a small signal at 33 ppm due to the  $\text{AlL}_5^{\text{NF}}$  was already present in the NMR spectrum even before the pretreatment, and it increased considerably after treatment. The authors attributed these coordinatively unsaturated, nonframework  $\text{AlL}_5^{\text{NF}}$  species to both electron accepting as well as Lewis acid sites. Since introduction of oxygen into the aniline-adsorbed, pretreated zeolite samples caused either an increase (HM) or the generation (HY) of the ESR signal of aniline cation radical, the oxygen coordinated  $\text{O}_2\text{-AlL}_5^{\text{NF}}$  was suggested to be the true electron acceptor in zeolites, i.e.



Consistent with the important role of aluminum species (either framework or nonframework) as electron acceptors, an increase of the number of electron-accepting sites in zeolites was observed with decreased silicon to aluminum ratios.<sup>94,96</sup> Furthermore, the oxidizing power of zeolites was also pointed out to be an important basis for the cracking of hydrocarbons over zeolite catalysts, no matter what the true acid sites might be.<sup>108</sup>

In special cases where powerful electron donors are applied to zeolites, the trapped electrons in some zeolite frameworks can be envisaged in the form of ionic clusters of alkali metal cations. Thus, when sodium is deliberately evaporated into the fully sodium ion exchanged A,<sup>109</sup> X,<sup>110</sup> Y,<sup>109-112</sup> and sodalite,<sup>113</sup> which have repeating sodalite units as the basic building structure of the framework, the released electrons from the adsorbed sodium atoms have been shown to be effectively stabilized by forming ionic species such as  $\text{Na}_4^{3+}$  (in A, Y, sodalite) or  $\text{Na}_6^{5+}$  (in X) within sodalite units. Evaporation of related alkali metals such as potassium and rubidium into sodium ion exchanged Y also led to the formation of sodium ionic clusters,<sup>109,111</sup> confirming the electron transfer nature of the reactions, i.e.



$$(n = 4, 6; \text{M} = \text{Na, K, Rb})$$



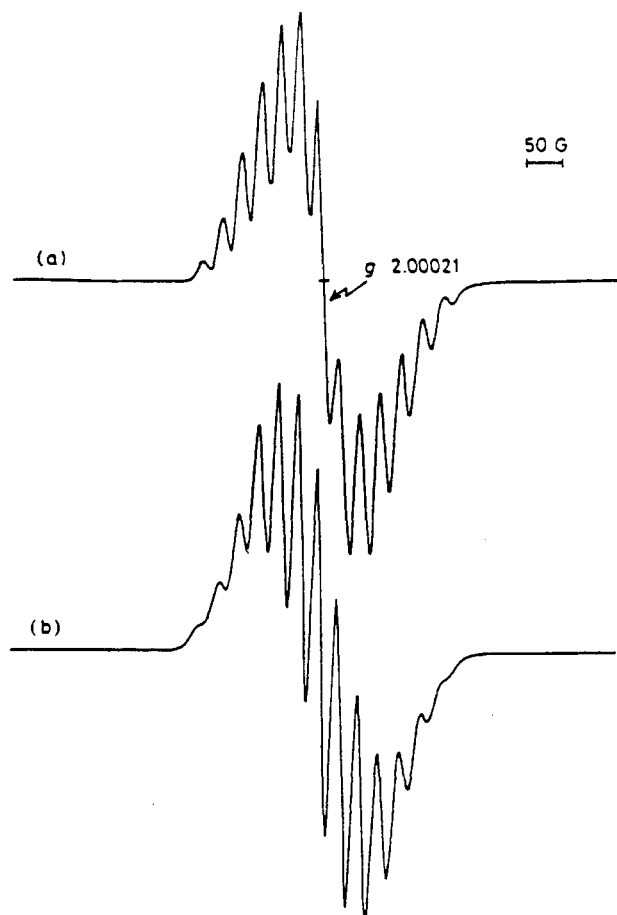


Figure 17. (a) ESR spectrum of  $\text{Na}_4^{3+}$  from the reduction of sodium zeolite-X by *n*-butyllithium in hexane at room temperature. (b) Simulated spectrum.<sup>118</sup>

Similarly the formation of  $\text{K}_3^{2+}$ ,  $\text{K}_4^{3+}$ ,  $\text{Cs}_4^{3+}$ ,  $\text{AB}_3^{3+}$  (A: alkali, B: alkali, alkaline earth, rare earth), and even  $\text{Ag}_4^{3+}$  has been reported.<sup>109,111,112,114</sup>

Sodium azide could be applied as the source of sodium atoms by the direct pyrolysis within zeolite-Y.<sup>115-117</sup> Organolithium compounds were also effectively used as the reductants for zeolites.<sup>118</sup> Thus the formation of sodium ionic clusters within zeolite-X in large quantities was conveniently achieved by merely immersing dried sodium zeolite-X into a hexane solution of *n*-butyllithium at room temperature under an argon atmosphere. Figure 17 represents the ESR spectrum of the brilliant purple zeolite-X obtained by this method consisting of 13 hyperfine splitting due to  $\text{Na}_4^{3+}$  with  $g = 2.004$  and  $a_{\text{Na}} = 29$  G. The same method could be applied to NaY and NaA. Interestingly, the reaction was facilitated when the zeolite were doped with small amounts of  $\text{Co}^{2+}$  ion. With the less electropositive phenyllithium as the reductant, the formation of ionic sodium clusters was only induced by UV irradiation ( $\lambda = 350$  nm) of the ethereal slurry of NaX containing phenyllithium.

Recently, a time-resolved diffuse reflectance spectroscopic study demonstrated that the electrons ejected from the photochemically excited arenes could induce the formation of sodium ionic clusters as the transient species.<sup>119</sup> Thus when arenes such as anthracene and pyrene that were intercalated within zeolite-X and Y were irradiated at 337 nm with a nitrogen laser, a broad transient absorption with  $\lambda_{\text{max}}$  at around 550 nm arose

together with the characteristic absorption bands due to cation radicals of the corresponding arenes. The 550-nm band was assigned to be that of  $\text{Na}_4^{3+}$  from comparison with literature data.<sup>120</sup> The transient absorptions did not decay to the baseline even on a millisecond time scale.

## 2. Radiation-Induced Acceptor Property

The simultaneous generation of positive hole centers and electrons on zeolites which were irradiated in vacuo with either  $\gamma$ - or X-rays has been known for a long time.<sup>121</sup> The generated electrons tend to be trapped at the aluminum center in the decationized zeolites giving six lines in the ESR spectrum,<sup>79,121</sup> or in the form of ionic sodium clusters<sup>120</sup> in the sodium ion exchanged zeolites (X and Y), giving 13 or 19 lines in the ESR spectra. The hole centers have been demonstrated to possess highly positive redox potentials. Accordingly, a variety of organic molecules such as aromatic compounds,<sup>122,123</sup> alkanes,<sup>124,125</sup> and even *trans*-2,3-dimethylethylene oxide,<sup>125</sup> which has a relatively high oxidation potential (9.88 eV), could be transformed into the corresponding monomeric cation radicals upon irradiation. Since zeolite pores have remarkable stabilizing properties for organic cation radicals<sup>96</sup> despite the much weaker cation radical-host interaction than is found in frozen alkyl halide and xenon matrices, the systematic use of zeolites as the most suitable media for the generation and spectroscopic characterization of a variety of organic cation radicals was proposed.<sup>96,99,125</sup>

## B. Zeolite Framework as Electron Donor

### 1. Induction by Thermal Treatment

In contrast with a variety of examples where zeolites served as effective and practically useful electron acceptors for many important organic and inorganic transformations, many fewer examples have been reported so far where zeolites acted as electron donors. Nevertheless, the electron-donating property of zeolites has long been verified by the ready formation of anion radicals of trinitrobenzene<sup>10,12</sup> and tetracyanoethylene<sup>12,13</sup> in zeolites, by merely immersing (thermally treated) zeolites in solutions of the compounds at ambient temperature. The formation of inorganic anion radicals, such as  $\text{SO}_2^{\cdot-}$ ,<sup>13,126</sup> has also been demonstrated by heating zeolites in the presence of the gas.  $\text{MV}^{2+}$ - or  $\text{DQ}^{2+}$ -exchanged zeolites usually begin to turn blue or green, respectively, during evacuation at moderately high temperatures ( $>100$  °C), indicating an electron transfer from zeolite frameworks to the bipyridinium acceptors.<sup>127</sup>

### 2. Radiation-Induced Donor Property

Irradiation ( $\gamma$ - or X-rays) of zeolites with adsorbed substrates has been widely applied for the formation of otherwise unstable anion radicals, stabilized by the zeolite cages.<sup>128</sup> The formation of superoxide and other unstable inorganic anion radicals has been extensively studied and reviewed.<sup>79,120,129-131</sup> Photoirradiation of alkaline earth metal ion exchanged zeolites with a xenon arc lamp in the presence of oxygen also generated superoxide ions.<sup>132</sup> In particular,  $\gamma$ -irradiation of silver ion exchanged zeolites has drawn some attention. The

formation of the polynuclear silver cluster  $\text{Ag}_6^+$ , which is surrounded by eight  $\text{Ag}^+$  ions in zeolite-A, has been studied by X-ray crystallography<sup>133</sup> and ESR.<sup>134</sup> The initial  $\gamma$ -irradiated product at 77 K was claimed to be an  $\text{Ag}_3^{2+}$  species, which upon annealing converted to the hexamer. The formation and stabilization of even silver atoms in zeolite-A and X was also studied.<sup>135</sup>

## V. Acknowledgments

I am grateful to Professor Jay K. Kochi at the University of Houston, Texas, who first stimulated and encouraged my interest in electron- and charge-transfer reactions within zeolites. I would like to express many thanks to all of my colleagues in the chemistry department of Sogang University for their generous help to continue the related research. The invaluable comments and suggestions made by all the referees are gratefully acknowledged. I also thank Professor William T. Miller at Regis University, Denver, Colorado, for his reading and commenting on the initial manuscript, and Y. S. Park and T. J. Huh for their help in preparing the figures and tables.

## VI. References

- (1) (a) Mulliken, R. S.; Person, W. B. *Molecular Complexes: A Lecture and Reprint Volume*; Wiley: New York, 1969. (b) Kosower, E. M. *Adv. Phys. Org. Chem.* **1965**, *3*, 81.
- (2) (a) Davidson, R. S. In *Molecular Association*; Foster, R., Ed.; Academic: New York, 1975, Vol. 1. (b) Davidson, R. S. *Adv. Phys. Org. Chem.* **1983**, *19*, 1. (c) Kochi, J. K. *Acta Chem. Scand.* **1990**, *44*, 409.
- (3) (a) Fox, M. A.; Chanon, M., Eds. *Photoinduced Electron Transfer*; Elsevier: New York, 1988. (b) Ebersson, L. *Electron Transfer Reactions in Organic Chemistry*; Springer-Verlag: Berlin, 1987.
- (4) (a) Foster, R., Ed. *Molecular Complexes*; Crane: New York, 1974; Vols. 1 and 2. (b) Andrews, L. J.; Keefer, R. M. *Molecular Complexes in Organic Chemistry*; Holden-Day: San Francisco, 1964.
- (5) Reichardt, C. *Solvent Effects in Organic Chemistry*; Verlag Chemie: Weinheim, Germany, 1979.
- (6) (a) Ramamurthy, V., Ed. *Photochemistry in Organized and Constrained Media*; VCH: New York, 1991. (b) Holt, S. L., Ed. *Inorganic Reactions in Organized Media*, ACS Symposium Series, No. 177; American Chemical Society: Washington, DC, 1981.
- (7) (a) Breck, D. W. *Zeolite Molecular Sieves*; Wiley: New York, 1974. (b) Barrer, R. M. *Hydrothermal Chemistry of Zeolites*; Academic: London, 1982. (c) Chen, N. Y.; Garwood, W. E.; Dwyer, F. G. *Shape Selective Catalysis in Industrial Applications*; Marcel Dekker: New York, 1989.
- (8) (a) Rabo, J. A.; Kasai, P. H. *Prog. Solid State Chem.* **1975**, *9*, 1. (b) Dutta, P. K.; Turbeville, W. *J. Phys. Chem.* **1991**, *95*, 4087.
- (9) Csicsery, S. M. In *Zeolite Chemistry and Catalysis*; Rabo, J. A., Ed.; ACS Monograph 171; American Chemical Society: Washington, DC, 1976; p 680 ff.
- (10) Turkevich, J.; Ono, Y. *Adv. Catal.* **1969**, *20*, 135.
- (11) Ono, Y.; Tokunaga, H.; Keii, T. *J. Phys. Chem.* **1975**, *79*, 752.
- (12) Flockart, B. D.; McLoughlin, L.; Pink, R. C. *J. Catal.* **1972**, *25*, 305.
- (13) Khulbe, K. C.; Mann, R. S.; Manoogian, A. *Zeolites* **1983**, *3*, 360.
- (14) Yoon, K. B.; Kochi, J. K. *J. Am. Chem. Soc.* **1989**, *111*, 1128.
- (15) Yoon, K. B.; Kochi, J. K. *J. Phys. Chem.* **1991**, *95*, 3780.
- (16) It has been suggested that 100 °C is not high enough to remove water completely from the zeolite cavities. However, at higher temperatures the acceptors are usually unstable. Therefore, the doped zeolites were washed briefly with methanol prior to evacuation.
- (17) (a) Mulliken, R. S. *J. Am. Chem. Soc.* **1950**, *72*, 601. (b) Mulliken, R. S.; Person, W. B. *Molecular Complexes*; Wiley: New York, 1969.
- (18) Calculated from normal C-C and C-H bond distances and angles plus 0.8 Å for the extra van der Waals radius of hydrogen.
- (19) Yoon, K. B.; Huh, T. J.; Kochi, J. K.; Corbin, D. R., manuscript in preparation.
- (20) Summers, L. A. *The Bipyridinium Herbicides*; Academic: New York, 1980.
- (21) Pal, M.; Bagghi, S. *J. Chem. Soc., Faraday Trans. 1* **1985**, *81*, 961.
- (22) Beaumont, T. G.; Davis, K. M. C. *J. Chem. Soc. B* **1968**, 1010.
- (23) (a) Kosower, E. M. *J. Org. Chem.* **1964**, *29*, 956. (b) Kosower, E. M.; Klinedinst, P. E. *J. Am. Chem. Soc.* **1956**, *78*, 3493. (c) Kosower, E. M. *J. Am. Chem. Soc.* **1958**, *80*, 3253. (d) Harmon, K. M.; Cummings, F. E.; Davis, D. A.; Diestler, D. J. *J. Am. Chem. Soc.* **1962**, *84*, 120, 3349.
- (24) Yoon, K. B.; Kochi, J. K. *J. Phys. Chem.* **1991**, *95*, 1348.
- (25) After prolonged standing with TBA<sup>+</sup>I<sup>-</sup> the weakly colored MVY and DQY were observed as pale yellow (1 week) and orange (1 day) powders, respectively.
- (26) Davis, K. M. C. In *Molecular Association*; Foster, R., Ed.; Academic: London, 1975; Vol. 1, p 151 ff.
- (27) Foster, R. *Organic Charge Transfer Complexes*; Academic: London, 1969; p 62 ff.
- (28) See Mauzerall, D. C., in ref 3a, Part A, Chapter 6, p 228 ff.
- (29) Sankararaman, S.; Yoon, K. B.; Yabe, T.; Kochi, J. K. *J. Am. Chem. Soc.* **1991**, *113*, 1419.
- (30) Dutta, P. K.; Incavo, J. A. *J. Phys. Chem.* **1987**, *91*, 4443.
- (31) Incavo, J. A.; Dutta, P. K. *J. Phys. Chem.* **1990**, *94*, 3075.
- (32) Faulkner, L. R.; Suib, S. L.; Renschler, C. L.; Green, J. M.; Bross, P. R. In *Chemistry in Energy Production*; Wymer, R. G., Keller, O. L., Eds.; American Chemical Society: Washington, DC, 1982; ACS Symposium Series; p 99 ff.
- (33) Persaud, L.; Bard, A. J.; Campion, A.; Fox, M. A.; Mallouk, T. E.; Webber, S. E.; White, J. M. *J. Am. Chem. Soc.* **1987**, *109*, 7309.
- (34) Krueger, J. S.; Mayer, J. E.; Mallouk, T. E. *J. Am. Chem. Soc.* **1988**, *110*, 8232.
- (35) Kim, Y. I.; Mallouk, T. E. *J. Phys. Chem.* **1992**, *96*, 2879.
- (36) (a) Wilkinson, F.; Willsher, C. J.; Casal, H. L.; Johnston, L. J.; Scaiano, J. C. *Can. J. Chem.* **1986**, *64*, 539. (b) Wilkinson, F.; Willsher, C. J. *Tetrahedron* **1987**, *43*, 1197. (c) Casal, H. L.; Scaiano, J. C. *Can. J. Chem.* **1985**, *63*, 1308.
- (37) (a) Ramamurthy, V.; Corbin, D. R.; Johnston, L. J. *J. Am. Chem. Soc.* **1992**, *114*, 3870. (b) Ramamurthy, V.; Caspar, J. V.; Corbin, D. R.; Eaton, D. F. *Photochem. Photobiol.* **1990**, *51*, 259.
- (38) (a) Kazanis, S.; Azarani, A.; Johnston, L. J. *J. Phys. Chem.* **1991**, *95*, 4431. (b) Drake, J. M.; Levitz, P.; Turro, N. J.; Nitsche, K. S.; Cassidy, K. F. *J. Phys. Chem.* **1988**, *92*, 4680.
- (39) Also see: (a) Wilkinson, F.; Willsher, C. J.; Leicester, P. A.; Barr, J. R. M.; Smith, M. J. C. *J. Chem. Soc., Chem. Commun.* **1986**, 1216. (b) Wilkinson, F. *J. Chem. Soc., Faraday Trans. 2* **1986**, *82*, 2073. (c) Wilkinson, F.; Willsher, C. J. *Appl. Spec.* **1984**, *38*, 6. (d) Kessler, R. W.; Wilkinson, F. *J. Chem. Soc., Faraday Trans. 1* **1981**, 77.
- (40)  $\lambda_{\text{max}}$ (CT) of the Naph-MV<sup>2+</sup> complex at the ground state was 390 nm.
- (41) (a) De Wilde, W.; Peeter, G.; Lunsford, J. H. *J. Phys. Chem.* **1980**, *84*, 2306. (b) Quayle, W. H.; Peeters, G.; De Roy, G. L.; Vansant, E. F.; Lunsford, J. H. *Inorg. Chem.* **1982**, *21*, 2226.
- (42) Bock, C. R.; Meyer, T. J.; Whitten, D. G. *J. Am. Chem. Soc.* **1974**, *96*, 4710.
- (43) Kalyanasundaram, K.; Kiwi, J.; Grätzel, M. *Helv. Chim. Acta* **1978**, *61*, 2720.
- (44) Ghosh, P. K.; Bard, A. J. *J. Phys. Chem.* **1984**, *88*, 5519.
- (45) Colon, J. L.; Yang, C.; Clearfield, A.; Martin, C. R. *J. Phys. Chem.* **1990**, *94*, 874.
- (46) Kalyanasundaram, K. *Coord. Chem. Rev.* **1982**, *46*, 159.
- (47) (a) Li, Z.; Mallouk, T. E. *J. Phys. Chem.* **1987**, *91*, 643. (b) de Vismes, B.; Bedioui, F.; Devynek, J.; Bied-Charreton, C. *J. Electroanal. Chem.* **1985**, *187*, 197.
- (48) (a) Sawyer, D. T.; Valentine, J. S. *Acc. Chem. Res.* **1981**, *14*, 393. (b) Wilshire, J.; Sawyer, D. T. *Acc. Chem. Res.* **1979**, *12*, 105.
- (49) Kasai, P. H.; Bishop, R. J., Jr. *J. Phys. Chem.* **1973**, *77*, 2308.
- (50) (a) Fedtke, C. *Biochemistry and Physiology of Herbicidal Action*; Springer-Verlag: Berlin, 1982. (b) Rabinowitch, H. D.; Fridovich, I. *Photochem. Photobiol.* **1983**, *37*, 679. (c) Krall, J.; Bagley, A. C.; Mullenbach, G. T.; Hallewell, R. A.; Lynch, E. R. *J. Biol. Chem.* **1988**, *263*, 1910.
- (51) (a) Harbour, J. R.; Bolton, J. R. *Biochem. Biophys. Res. Commun.* **1975**, *64*, 803. (b) Chia, L. S.; McRae, D. G.; Thompson, J. E. *Physiol. Plant* **1982**, *56*, 492. (c) Sinha, B. K.; Singh, Y.; Krishna, G. *Biochem. Biophys. Res. Commun.* **1986**, *135*, 583.
- (52) (a) Epel, B. L.; Neumann, J. *Biochim. Biophys. Acta* **1973**, *325*, 520. (b) Youngman, R. J.; Dodge, A. D. *Z. Naturforsch.* **1979**, *34C*, 1032. (c) Farrington, J. A.; Ebert, M.; Land, E. J.; Fletcher, K. *Biochim. Biophys. Acta* **1973**, *314*, 372.
- (53) Yoon, K. B.; Kochi, J. K. *J. Am. Chem. Soc.* **1988**, *110*, 6586.
- (54) Herron, N. *Inorg. Chem.* **1986**, *25*, 4714.
- (55) Vansant, E. F.; Lunsford, J. H. *Adv. Chem. Ser.* **1973**, *121*, 441.
- (56) Howe, R. F.; Lunsford, J. H. *J. Am. Chem. Soc.* **1975**, *97*, 5156.
- (57) Schoonheydt, R. A.; Delgrims, J. *J. Chem. Soc. Dalton Trans.* **1981**, 915.
- (58) Howe, R. F.; Lunsford, J. H. *J. Phys. Chem.* **1975**, *79*, 1836.
- (59) Mizuno, K.; Imamura, S.; Lunsford, J. H. *Inorg. Chem.* **1984**, *23*, 3510.
- (60) (a) Drago, R. S.; Bresinska, I.; George, J. E.; Balkus, K. J., Jr.; Taylor, R. J. *J. Am. Chem. Soc.* **1988**, *110*, 304. (b) Taylor, R. J.; Drago, R. S.; George, J. E. *J. Am. Chem. Soc.* **1989**, *111*, 6610.
- (61) Ono, Y.; Suzuki, K.; Keii, T. *J. Phys. Chem.* **1974**, *78*, 218.
- (62) Kuznicki, S. M.; Devries, K. L.; Eyring, E. M. *J. Phys. Chem.* **1980**, *84*, 535.

- (63) Kellerman, R.; Hutta, P. J.; Klier, K. *J. Am. Chem. Soc.* **1974**, *96*, 5946.
- (64) Rabo, J. A.; Angell, C. L.; Kasai, P. H.; Schomaker, V. *Discuss. Faraday Soc.* **1966**, *41*, 328.
- (65) Ozin, G. A.; Godber, J. *J. Phys. Chem.* **1989**, *93*, 878.
- (66) Richardson, J. T. *J. Catal.* **1967**, *9*, 172.
- (67) Slikin, A. A.; Loktev, M. I.; Mishin, I. V.; Plakhotnik, V. A.; Klyachko, A. L.; Rubinstejn, A. M. *Kinet. Katal.* **1979**, *20*, 181.
- (68) (a) Chon, H.; Seo, G.; Ahn, B. *J. J. Catal.* **1983**, *80*, 90. (b) Seo, G.; Chon, H. *J. Catal.* **1981**, *67*, 424. (c) Hwang, B.; Chon, H. *Zeolites* **1990**, *10*, 101.
- (69) Leith, I. R.; Kemball, C.; Leach, H. F. *Chem. Commun.* **1971**, 407.
- (70) Enzel, P.; Bein, T. *J. Chem. Soc., Chem. Commun.* **1989**, 1326.
- (71) Chao, T. H.; Erf, H. A. *J. Catal.* **1986**, *100*, 492.
- (72) Liu, H.; Shen, W.; Quayle, W. H.; Lunsford, J. H. *Inorg. Chem.* **1984**, *23*, 4553.
- (73) Calzaferri, G.; Suter, W.; Waldeck, B. *J. Chem. Soc., Chem. Commun.* **1990**, 485.
- (74) Jermyn, J. W.; Johnson, T. J.; Vansant, E. F.; Lunsford, J. H. *J. Phys. Chem.* **1973**, *77*, 2964.
- (75) Naccache, C.; Ben Taarit, Y. *J. Chem. Soc. Faraday Trans. I* **1973**, *69*, 1475.
- (76) Kasai, P. H.; Bishop, R. J., Jr. *J. Am. Chem. Soc.* **1972**, *94*, 5560.
- (77) Barrer, R. M.; Whiteman, J. L. *J. Chem. Soc. A* **1967**, 19.
- (78) Stamires, D. N.; Turkevich, J. *J. Am. Chem. Soc.* **1964**, *86*, 749.
- (79) Dollish, F. R.; Hall, W. K. *J. Phys. Chem.* **1967**, *71*, 1005.
- (80) Hirschler, A. E.; Neikam, W. C.; Barmby, D. S.; James, R. L. *J. Catal.* **1965**, *4*, 628.
- (81) Chen, F. R.; Fripiat, J. J. *J. Phys. Chem.* **1992**, *96*, 819.
- (82) Corio, P. L.; Shih, S. *J. Catal.* **1970**, *18*, 126.
- (83) Sagert, N. H.; Pouteau, R. M. L.; Bailey, M. G.; Sargent, F. P. *Can. J. Chem.* **1972**, *50*, 2041.
- (84) Tokunaga, H.; Ono, Y.; Keii, T. *Bull. Chem. Soc. Jpn.* **1973**, *46*, 3569.
- (85) Kurita, Y.; Sonoda, T.; Sato, M. *J. Catal.* **1970**, *19*, 82.
- (86) Vadrine, J. C.; Auroux, A.; Bolis, V.; Dejaifve, P.; Naccache, C.; Wierzchowski, P.; Derouane, E. G.; Nagy, J. B.; Gilson, J.-P.; van Hooff, J. H. C.; van den Berg, J. P.; Wolthuizen, J. *J. Catal.* **1979**, *59*, 248.
- (87) Slinkin, A. A.; Kucherov, A. V.; Kondrat'ev, D. A.; Bondarenko, T. N.; Rubinshtein, A. M.; Minachev, Kh. M. *J. Mol. Catal.* **1986**, *35*, 97.
- (88) Bolshov, V. A.; Volodin, A. M. *React. Kinet. Catal. Lett.* **1991**, *43*, 87.
- (89) Shih, S. *J. Catal.* **1983**, *79*, 390.
- (90) Rhodes, C. J. *J. Chem. Soc. Faraday Trans.* **1991**, *87*, 3179.
- (91) Chen, F.; Guo, X. *J. Chem. Soc., Chem. Commun.* **1989**, 1682.
- (92) Shih, S. *J. Phys. Chem.* **1975**, *79*, 2201.
- (93) Lange, J.-P.; Gutsze, A.; Karge, H. G. *J. Catal.* **1988**, *114*, 136.
- (94) Karge, H. G.; Lange, J.-P.; Gutsze, A.; Laniecki, M. *J. Catal.* **1988**, *114*, 144.
- (95) Suib, S. L.; McMahon, K. C.; Psaras, D. In *Intrazeolite Chemistry*; Stucky, G. D., Dwyer, F. G., Eds.; ACS Symposium Series 218; American Chemical Society, Washington, DC, 1983; p 301 ff.
- (96) Ramamurthy, V.; Caspar, J. V.; Corbin, D. R. *J. Am. Chem. Soc.* **1991**, *113*, 594.
- (97) (a) Shida, T.; Hamill, W. H. *J. Phys. Chem.* **1966**, *44*, 4372. (b) Shida, T.; Hamill, W. H. *Ibid.* **1966**, *44*, 2375.
- (98) (a) Almgreen, M.; Thomas, J. K. *Photochem. Photobiol.* **1980**, *31*, 329. (b) Ebbeson, T. *J. Phys. Chem.* **1988**, *92*, 4581. (c) Goodman, J. L.; Peters, K. *J. Am. Chem. Soc.* **1985**, *107*, 6459. (d) Lewis, F. L.; Dykstra, R. E.; Gould, I. R.; Farid, S. *J. Phys. Chem.* **1988**, *92*, 7042. (e) Oelkrug, D.; Krabichler, G.; Honnen, W.; Wilkinson, F.; Willsher, C. *J. Phys. Chem.* **1988**, *92*, 3589.
- (99) Caspar, J. V.; Ramamurthy, V.; Corbin, D. R. *J. Am. Chem. Soc.* **1991**, *113*, 600.
- (100) Enzel, P.; Bein, T. *J. Phys. Chem.* **1989**, *93*, 6270.
- (101) Heaviside, J.; Hendra, P. J.; Tsai, P.; Cooney, R. P. *J. Chem. Soc. Faraday Trans. 1* **1978**, *74*, 2542.
- (102) Dutta, P. K.; Puri, M. *J. Catal.* **1988**, *111*, 453.
- (103) Ghosh, S.; Bauld, N. L. *J. Catal.* **1985**, *95*, 300.
- (104) Lorenz, K.; Bauld, N. L. *J. Catal.* **1985**, *95*, 613.
- (105) Bauld, N. L. *Tetrahedron* **1989**, *45*, 5307.
- (106) Lombardo, E. A.; Hall, W. K. *J. Catal.* **1988**, *112*, 565.
- (107) Kerr, G. T. *J. Phys. Chem.* **1967**, *71*, 4155.
- (108) (a) McVicker, G. B.; Kramer, G. M.; Ziemiak, J. J. *J. Catal.* **1983**, *83*, 286. (b) McVicker, G. B.; Kramer, G. M.; Ziemiak, J. J. *J. Catal.* **1985**, *92*, 355.
- (109) Harrison, M. R.; Edwards, P. P.; Klinowski, J.; Thomas, J. M.; Johnson, D. C.; Page, C. J. *J. Solid State Chem.* **1984**, *54*, 330.
- (110) Rabo, J. A.; Angell, C. L.; Kasai, P. H.; Schomaker, V. *Discuss. Faraday Soc.* **1966**, *41*, 328.
- (111) Edwards, P. P.; Harrison, M. R.; Klinowski, J.; Ramdas, S.; Thomas, J. M.; Johnson, D. C.; Page, C. J. *J. Chem. Soc., Chem. Commun.* **1984**, 982.
- (112) Westphal, U.; Geismar, G. Z. *Anorg. Allg. Chem.* **1984**, *508*, 165.
- (113) Smeulders, J. B. A. F.; Hefni, M. A.; Klaassen, A. A. K.; de Boer, E.; Westphal, U.; Geismar, G. *Zeolites* **1987**, *7*, 347.
- (114) (a) Xu, B.; Chen, X.; Kevan, L. *J. Chem. Soc. Faraday Trans.* **1991**, *87*, 3157. (b) Xu, B.; Kevan, L. *Ibid.* **1991**, *87*, 3157. (c) Xu, B.; Kevan, L. *J. Phys. Chem.* **1991**, *95*, 1147.
- (115) Martens, L. R. M.; Grobet, P. J.; Jacobs, P. A. *Nature* **1985**, *315*, 568.
- (116) Martens, L. R. M.; Grobet, P. J.; Vermeiren, W. J. M.; Jacobs, P. A. *Proc. 7th Int. Zeolite Conf.* **1986**, 935.
- (117) Martens, L. R. M.; Vermeiren, W. J. M.; Grobet, P. J.; Jacobs, P. A. *Stud. Surf. Sci. Catal.* **1987**, *31*, 531.
- (118) Yoon, K. B.; Kochi, J. K. *J. Chem. Soc., Chem. Commun.* **1988**, 510.
- (119) (a) Iu, K.-K.; Thomas, J. K. *J. Phys. Chem.* **1991**, *95*, 506. (b) Iu, K.-K.; Thomas, J. K. *Colloids Surf.* **1992**, *63*, 39.
- (120) Kasai, P. H. *J. Chem. Phys.* **1965**, *43*, 3322.
- (121) Stamires, D. N.; Turkevich, J. *J. Am. Chem. Soc.* **1964**, *86*, 757.
- (122) Komatsu, T.; Lund, A. *J. Phys. Chem.* **1972**, *76*, 1727.
- (123) Komatsu, T.; Lund, A.; Kinell, P. O. *J. Phys. Chem.* **1972**, *76*, 1721.
- (124) Toriyama, K.; Nunome, K.; Iwasaaki, M. *J. Am. Chem. Soc.* **1987**, *109*, 4496.
- (125) Qin, X. Z.; Trifunac, A. D. *J. Phys. Chem.* **1990**, *94*, 4751.
- (126) Tokunaga, H.; Ono, Y.; Keii, T. *Bull. Chem. Soc. Jpn.* **1973**, *46*, 3362.
- (127) Yoon, K. B., unpublished result.
- (128) Kasai, P. H.; Bishop, R. J., Jr. In *Zeolite Chemistry and Catalysis*; Rabo, J. A., Ed., ACS Monograph 171; American Chemical Society: Washington, DC, 1976; Chapter 6.
- (129) Wang, K. M.; Lunsford, J. H. *J. Phys. Chem.* **1971**, *75*, 1165.
- (130) Lunsford, J. H. *Catal. Rev.* **1973**, *8*, 135.
- (131) Gardner, C. L.; Casey, E. *J. Catal. Rev.* **1974**, *9*, 1.
- (132) Chamulitrat, W.; Kevan, L. *J. Phys. Chem.* **1985**, *89*, 4989.
- (133) Kim, Y.; Seff, K. *J. Am. Chem. Soc.* **1978**, *100*, 6989.
- (134) Morton, J. R.; Preston, K. F. *Zeolites* **1987**, *7*, 2.
- (135) (a) Popovich, G. M.; Shekhobalova, V. I.; Malkin, A. I. *Russ. J. Phys. Chem.* **1983**, *57*, 1335. (b) Popovich, G. M.; Shekhobalova, V. I.; Malkin, A. I. *Ibid.* **1983**, *57*, 1338.